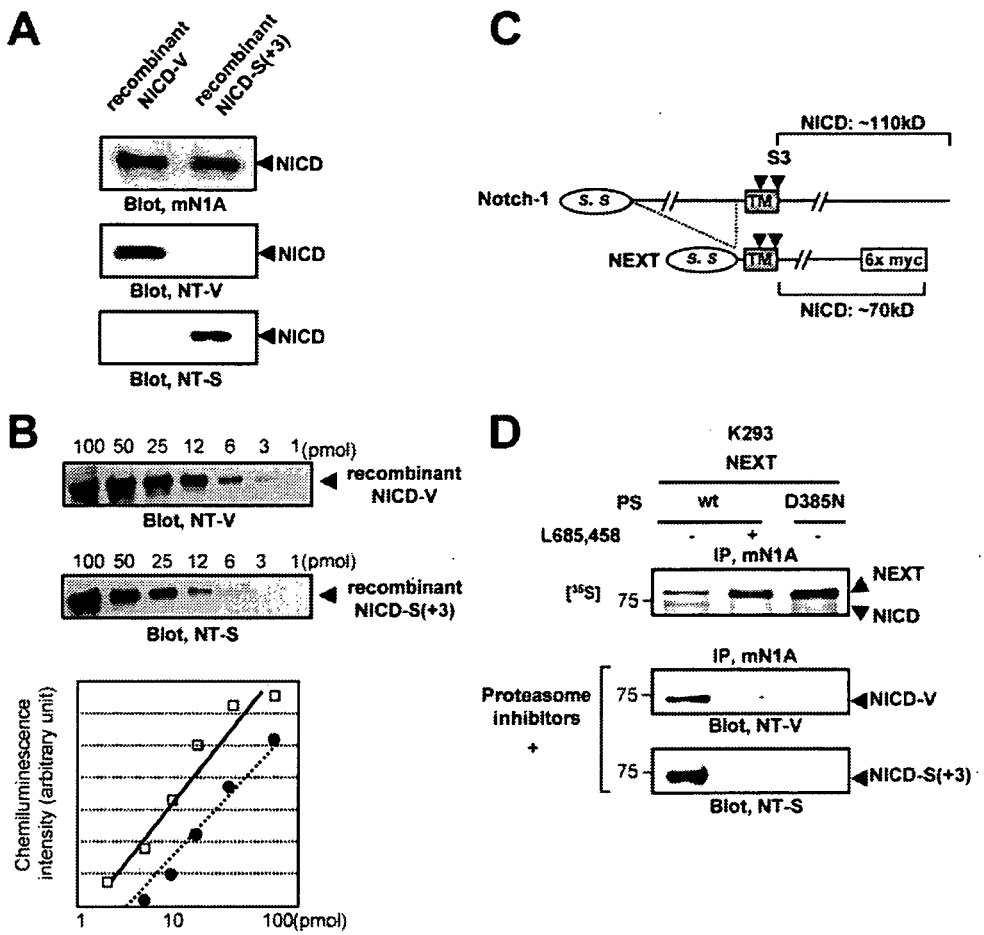

FIG. 2. Characterization of capping antibodies to the N terminus of NICD and detection of distinct NICD species in cultured cells. (A) Specificities of the anti-NT-V and the anti-NT-S antibodies. Immunoblotting with antibody mN1A confirmed that equal amounts of the polypeptides were loaded in each lane (upper panel). (B) Affinities of the anti-NT-V and anti-NT-S antibodies. The indicated amounts of NICD-V or NICD-S(+3) were separated by SDS-PAGE and analyzed by immunoblotting with the anti-NT-V or anti-NT-S antibody, respectively. The graph shows the chemiluminescence intensity versus the concentration of NICD-V (squares) or NICD-S(+3) (circles). Each antibody detected the respective polypeptide in a dose-dependent manner. (C) Schematic representation of Notch-1 and NEXT constructs. The C-terminal portion of the NEXT construct is replaced by myc_6, while full-length Notch-1 has no modification. Note that the molecular mass of NICD generated from NEXT-myc_6 is ~70 kDa, while that of NICD generated from unmodified Notch-1 is ~110 kDa. (D) Generation of NICD-V and NICD-S(+3) in cultured cells. Proteasome inhibitors lactacystin (10 μM), MG262 (100 nM), and NLVS (10 μM) were added to the medium 12 h prior to cell collection.

with distinct N termini (Fig. 2A; see Fig. S2A in the supplemental material). We found that (i) the anti-NT-V antibody specifically recognizes recombinant NICD-V but not NICD-S(+3) (34) (Fig. 2A, middle panel; see Fig. S2B in the supplemental material), whereas the anti-NT-S antibody has the opposite specificity (Fig. 2A; lower panel, see also Fig. S2B in the supplemental material), and (ii) these antibodies can be used to determine the relative amounts of NICD-V and NICD-S(+3) generated, that is, the extents of S3-V and S3-S(+3) cleavage, respectively (Fig. 2B).

Using these capping antibodies, we examined the diversity in the site of S3 cleavage in living cells. The Notch extracellular truncation (NEXT) (Fig. 2C), which lacks the majority of the extracellular domain of Notch-1, undergoes constitutive ligand-independent intramembrane proteolysis by PS/γ-secretase (24). We prepared cells stably expressing NEXT and wt or a dominant-negative form of PS1 (PS1 D385N) (51). A 30-min pulse with [^{35}S]methionine followed by a 2-h chase revealed production of an ~70-kDa NICD band that completely disappeared upon elimination of PS/γ-secretase function (Fig. 2D, upper panel). Because degradation of NICD is mediated by the ubiquitin-proteasome pathway (8, 40, 41), we added a potent proteasome inhibitor mixture consisting of lactacystin, MG262, and NLVS (Fig. 2D, middle and lower panels). The resulting cell lysates were immunoprecipitated with antibody mN1A, separated by SDS-PAGE, and analyzed by immunoblotting with anti-NT-V or anti-NT-S. The anti-NT-V and anti-NT-S antibodies specifically detected the PS-dependent production of NICD-V and NICD-S(+3), respectively (Fig. 2D, middle and lower panels; see Fig. S2C in the supplemental material). We also confirmed that both NICD-V and NICD-S(+3) are produced in cells in the absence of the proteasome inhibitor mixture (see Fig. S2D in the supplemental material).

S3 cleavage during Notch signaling produces distinct molecular species of NICD. Because ligand-induced degradation of Notch receptors is initiated at the plasma membrane (PM),

Downloaded from mcb.asm.org at Osaka University on March 12, 2008

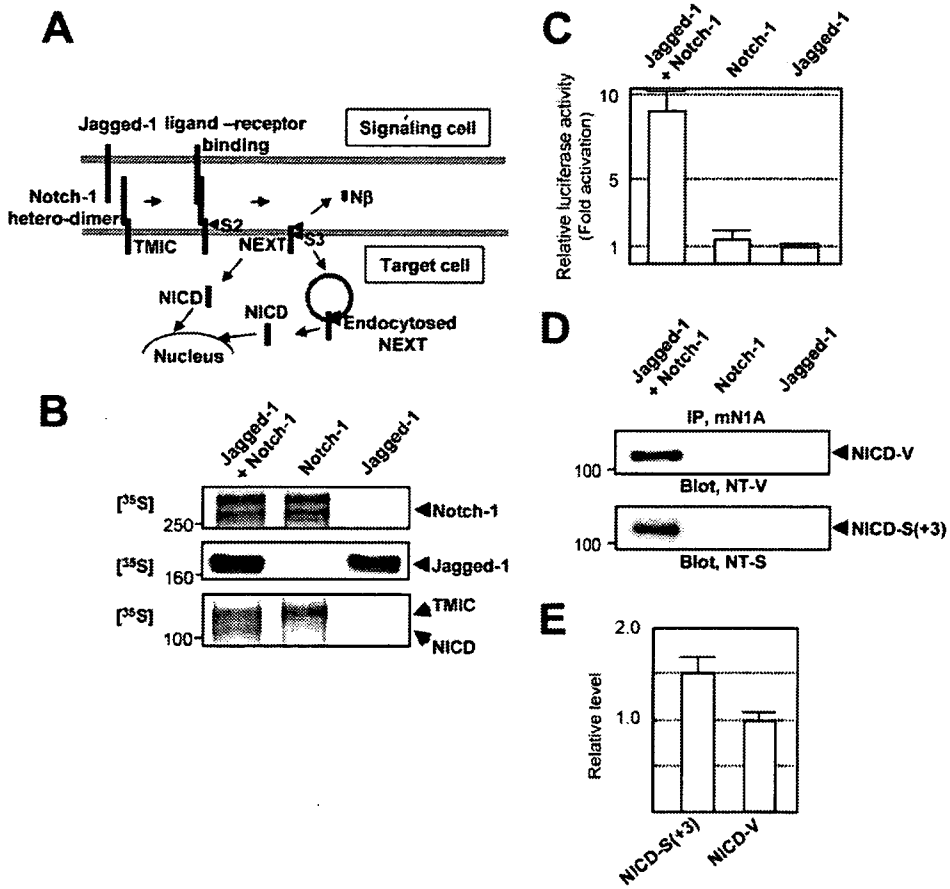

FIG. 3. Detection of different NICD species during Notch signaling. (A) Schematic representation of Notch signaling. (B) Notch signaling in cell culture. CHO(r) cells stably expressing Jagged-1 or Notch-1 were used. Expression of Notch-1 (top panel) and Jagged-1 (middle panel) was determined by a 1-h pulse experiment, followed by immunoprecipitation using antibodies mN1A and H114, respectively. The precipitated proteins were analyzed by SDS-PAGE, followed by autoradiography. A 1-h pulse/2-h chase experiment detected an ~110-kDa NICD band only when the cells were cocultured (bottom panel). (C) Notch signaling was measured using a dual luciferase assay. The relative luciferase activity of Jagged-expressing cells was defined as 1.0. Values represent means ± standard deviations (n = 3). (D) In the presence of the proteasome inhibitors, both NICD-V (upper panel) and NICD-S(+3) (lower panel) were detected during Notch signaling. The bands were detected as described for Fig. 2D. (E) Relative levels of NICD-S(+3) and NICD-V generated during Notch signaling. The relative levels were calculated based on the standard curve shown in Fig. 2B.

intramembrane proteolysis of Notch-1 is thought to occur at restricted subcellular locations, such as the PM and endocytosed vesicles (13, 17, 20) (Fig. 3A). We prepared cells stably expressing either Jagged-1 (a Notch ligand) or full-length Notch-1 and then cocultured them. We determined the extent of Notch signaling using a luciferase reporter assay in cells expressing a newly improved construct, *HES-Y* (see Materials and Methods for details). Pulse-chase experiments revealed that upon coculture, sequential endoproteolysis of Notch-1 occurs, producing the NICD band (Fig. 3B, bottom panel). Moreover, when the cells were cocultured, we observed concomitant activation of the *HES-1* promoter (Fig. 3C). The results therefore demonstrate Notch-1 signaling in cell culture. Using this assay system, we investigated whether NICD-S(+3) and NICD-V are indeed generated during Notch signaling. Strikingly, upon coculture, both NICD-V and NICD-S(+3) were detected (Fig. 3D, upper and lower panels). The intensities of the bands indicated that 1.5-fold more NICD-S(+3) than NICD-V was produced (Fig. 3E). Therefore, the results indicated that there are multiple forms of NICD produced during Notch signaling.

We next tried to detect the NICD-V and NICD-S(+3) in fetal (embryonic day 12, whole embryo without internal organs) and adult (brain) mouse tissues (Fig. 4). Nuclear extracts from these tissues were immunoprecipitated with mN1A, which specifically recognizes intracellular domain of Notch-1 but not Notch-2, -3, or -4. The precipitated proteins were then analyzed by SDS-PAGE, followed by immunoblotting with anti-NT-V or anti-NT-S antibodies. As shown in Fig. 4A, we clearly found both NICD-V (upper panel) and NICD-S(+3) species (lower panel) in the fetal mouse tissues, but these species were barely detectable in adult brains. This is consistent with the finding of a high level of Notch signaling in fetal mouse tissue (22). Moreover, we successfully detected the same NICD-V and NICD-S bands in the mouse embryo even when the combination of antibodies used for immunoprecipitation and immunoblotting was swapped (Fig. 4B). Therefore, the results indicated that multiple forms of NICD are produced in vivo.

Downloaded from mcb.asm.org at Osaka University on March 12, 2008

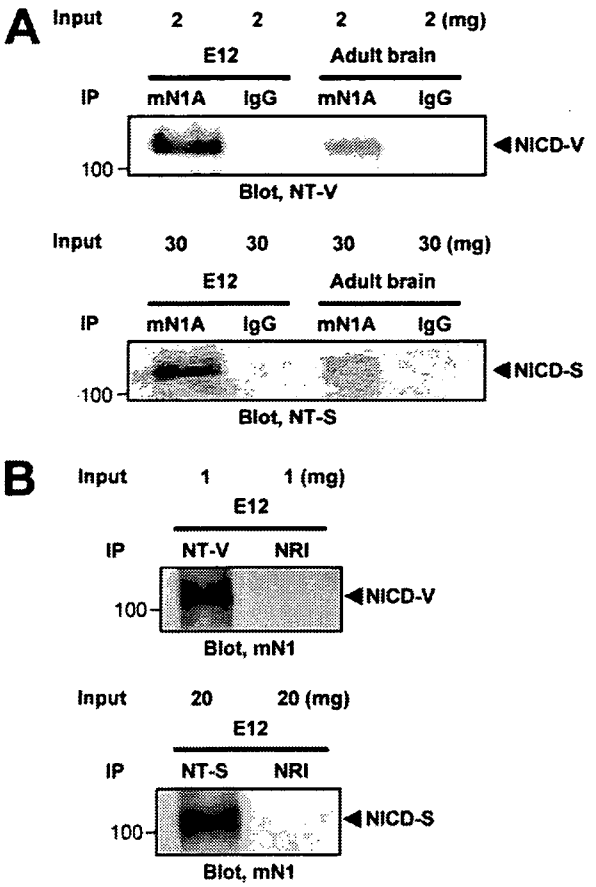

FIG. 4. Detection of NICD-V and NICD-S(+3) in vivo. The indicated amounts of nuclear extracts were loaded for immunoprecipitation. IgG and NRI, isotype-matched immunoglobulin and normal rabbit immunoglobulin, respectively.

Transactivation of the HES-1 promoter by NICD-S(+3) is much weaker than transactivation by NICD-V in living cells. The stability of polypeptides degraded by the ubiquitin-proteasome pathway depends on the N-end rule, where an N-terminal valine is a stabilizing residue and an N-terminal serine is destabilizing (2, 12). Therefore, we examined whether the intensity of Notch signaling differs for NICD-V and NICD-S(+3) in living cells. We loaded *HES-Y*-transfected cells with equal amounts of purified NICD-V or NICD-S(+3) (see Fig. S3 in the supplemental material). After a 1-h loading period, the cells contained similar levels of each NICD species (Fig. 5A). Induction of Notch signaling by chasing the loaded cells for 4 h (signaling period) resulted in much less luciferase activity in the NICD-S-loaded cells than in NICD-V-loaded cells, demonstrating that NICD-S(+3) is much weaker than NICD-V at activating the promoter in living cells (Fig. 5B, left panel).

We next investigated whether the rates of degradation by the proteasome pathway differ for the various species of NICD in an in vitro assay. We incubated recombinant NICD-V or NICD-S(+3) (34) with rabbit reticulocyte lysate (Promega) (12) and examined the levels of the two types of NICD by immunoblotting (Fig. 5C). Our results indicated that NICD-S(+3) is much less stable than NICD-V (Fig. 5D). Moreover, following the proteasome inhibitor treatment, the relative luciferase activities in NICD-S- and NICD-V-loaded cells turned out to be almost the same (Fig. 5E). Collectively the results suggest that unstable NICD-S(+3) may have a much weaker ability than stable NICD-V to mediate intracellular signaling.

The precision of S3 cleavage is distinct in the subcellular locations where it occurs. A previous study showed that the precision of ε cleavage of βAPP, which topologically corresponds to S3 cleavage of Notch-1, differs before and after endocytosis (11). To determine whether S3 cleavage precision differs on PM and endosomes, we performed the cell-free assay using organelles separated by iodixanol gradient fractionation from NEXTΔC-expressing HeLa cells (11). Fractions from a 2.5% to 25% linear iodixanol gradient were examined by immunoblotting with antibodies to early endosome antigen 1 (endosome marker), Na-K ATPase (PM marker), GM130 (Golgi marker), or nicastrin (a component of the PS complex) (Fig. 6A). NICD(ΔC) was generated in the cell-free assay using membranes collected by centrifugation from the endosome-rich (fraction 3) and the PM-rich (fraction 7) fractions and analyzed by immunoprecipitation/MALDI-TOF MS. Remarkably, the relative ratio of NICD-V(ΔC) to NICD-S(+3)(ΔC) was much higher in the PM-rich fraction than in the endosome-rich fraction (Fig. 6B). This indicates that cleavage at S3-V, which generates the longer NICD-V(ΔC), and at S3-S(+3), which generates the shorter NICD-S(+3)(ΔC), occurs predominantly on the PM and endosomes, respectively. This is very similar to the case of ε cleavage of βAPP (11). Subsequently, we investigated the effect of endocytosis on the precision of S3 cleavage. To down-regulate endocytosis, we used cells that express a dominant-negative mutant of dynamin-1 (Dyn-1 K44A) upon tetracycline withdrawal (Fig. 6C) or treatment with bafilomycin A1 (11) (see Fig. S4 in the supplemental material). When endocytosis was strongly inhibited, the precision of S3 cleavage changed drastically, so that the S3-V site instead of the S3-S(+3) site became the major site of cleavage in the cell-free assay (Fig. 6C; see Fig. S4A in the supplemental material). These results from the cell-free assay suggest that generation of stable NICD-V and unstable NICD-S occur predominantly on the PM and endosomes, respectively.

The precision of S3 cleavage changes in parallel with the rate of endocytosis in target cells. Next, we investigated whether these phenomena also occur in living cells. We examined the influence of the rate of endocytosis of NEXT by altering the expression of Dyn-1 K44A in living cells (Fig. 7A). Measurement of biotinylated transferrin uptake revealed various rates of endocytosis in Dyn-1 K44A-expressing cells (Fig. 7B). Strikingly, we found that the ratio of S3-V to S3-S(+3) is low in cells with a high rate of endocytosis and, conversely, that the ratio is high in cells with a low rate of endocytosis (Fig. 7C), which is consistent with the result from the cell-free assay (Fig. 6C). We observed a similar change in the S3 cleavage when endocytosis was blocked with bafilomycin A1 (see Fig. S4B in the supplemental material). Therefore, it appears that the precision of S3 cleavage changes in parallel with the rate of endocytosis, and relative generation of stable NICD-V increases as the rate of endocytosis decreases.

Because Notch signaling is associated with endocytosis of Notch receptors and/or Notch ligands during development (3, 28, 35, 40, 43), we next examined the effect of the change in S3

Downloaded from mcb.asm.org at Osaka University on March 12, 2008

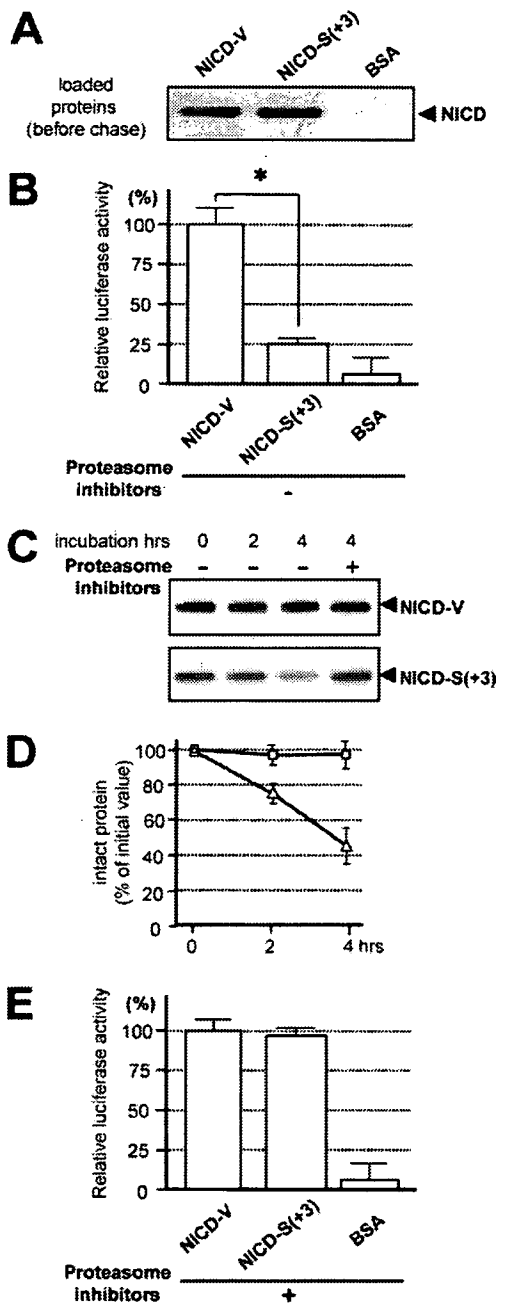

FIG. 5. Characterization of the NICD species. (A) Loading of cells with NICD. HeLa cells (2.5×10^5) were loaded with 5 μg of purified NICD-V, NICD-S(+3), or BSA (control). The cells were collected 1 h after the addition of the Chariot macromolecule complex (defined as the loading period). (B) Assay of Notch downstream signaling induced by the NICD species. The NICD-loaded cells from panel A were chased for 4 h and collected, and Notch downstream signaling was assayed. The values were corrected for background luciferase activity (0.5 μg of β-galactosidase-loaded cells), and the luciferase activity in the NICD-V-loaded cells was defined as 100%. Values represent means ± standard deviations ($n = 3$). The asterisk indicates that the relative luciferase activity in NICD-V-loaded cells is statistically different than that in NICD-S(+3)-loaded cells ($P < 0.001$). Similar results were obtained using cells expressing pGa981-6 (data not shown). (C) Stability of recombinant NICD species in rabbit reticulocyte lysate. Note that the degradation of NICD-S(+3) was inhibited in the presence of proteasome inhibitors. (D) Levels of intact NICDs in the lysates during in vitro degradation. The amount of intact polypeptide was determined using a standard curve of the chemiluminescence intensities of the bands versus their concentrations (data not shown). Squares and triangles indicate the means for NICD-V and NICD-S(+3), respectively. Values represent means ± standard deviations ($n = 3$). (E) Assay of Notch downstream signaling induced by the NICD species in the presence of the proteasome inhibitor mixture. Experiments were performed as described for panel B in the presence of the proteasome inhibitor mixture. The values were corrected for background luciferase activity (0.5 μg of β-galactosidase-loaded cells), and the luciferase activity in the NICD-V-loaded cells was defined as 100%. Values represent means ± standard deviations ($n = 3$).

precision on the intensity of Notch signaling. Surprisingly, we observed a higher intensity of Notch signaling in cells in which the rate of endocytosis of NEXT was lower (Fig. 7D; see Fig. S4C in the supplemental material). These results suggest that the rate of endocytosis in target cells could affect the intensity of intracellular Notch signaling by changing the precision of S3 cleavage and thus its stability.

Mutations around S3 can induce changes in the precision of the cleavage. S3 mutations, such as the Val→Gly mutation (V1744G mutant) and the Lys→Arg mutation (K1749R mutant), cause a decrease in the NICD level (13, 15). To date, this reduction has been considered to be due to decreased NICD generation. However, since we revealed that multiple NICD species with different stabilities are generated, we investigated whether these mutants also change the S3 cleavage precision, which would accelerate degradation of NICD. First, we determined the precision of the S3 cleavage of the Val→Gly mutant version of NEXTΔC in the cell-free assay (Fig. 1C). Strikingly, this mutant was degraded mainly into NICD-L(+1)(ΔC), which has Leu1745 (murine Notch-1 numbering) at its N terminus (Fig. 8A). Therefore, it appears that the Val→Gly mutation causes not only a complete loss of stable NICD-V, but also a dramatic shift in the major product from NICD-S(+3) to NICD-L(+1). We next examined whether NICD-L(+1) behaved like NICD-S(+3) in cellular signal transduction. Like NICD-S(+3), NICD-L(+1) was much weaker than NICD-V at inducing promoter activation in living cells (Fig. 8B). Moreover, our in vitro degradation assay revealed that NICD-L(+1) was much less stable than NICD-V (Fig. 8C). Thus, our in vitro experiments suggested that NICD-L(+1) and NICD-S(+3) are both unstable and have similar effects on Notch signaling but that their effects are distinct from those of NICD-V. We further investigated whether the precision change in the mutant is also observed in living cells. To specifically detect NICD-L(+1), we generated anti-NT-L, an N-terminal capping antibody (see Fig. S5 in the supplemental material). As is clearly shown in Fig. 8D, although almost no NICD-V was detected, a substantial amount of NICD-L(+1) was detected in the Val→Gly version of NEXT-expressing cells. These results indicate that the relative production of unstable NICDs with respect to stable NICD increases in the mutant NEXT cells due to change of the S3 cleavage precision.

The Lys→Arg mutant NEXT (the K1749R mutant) is neither monoubiquitinated nor endocytosed (13). This mutant, like the Val→Gly mutant, causes decreased NICD levels in cell culture (13). Analysis to determine the precision of the S3 cleavage of the Lys→Arg mutant version of NEXTΔC was performed in the cell-free assay. Surprisingly, the Lys→Arg

Downloaded from mcb.asm.org at Osaka University on March 12, 2008

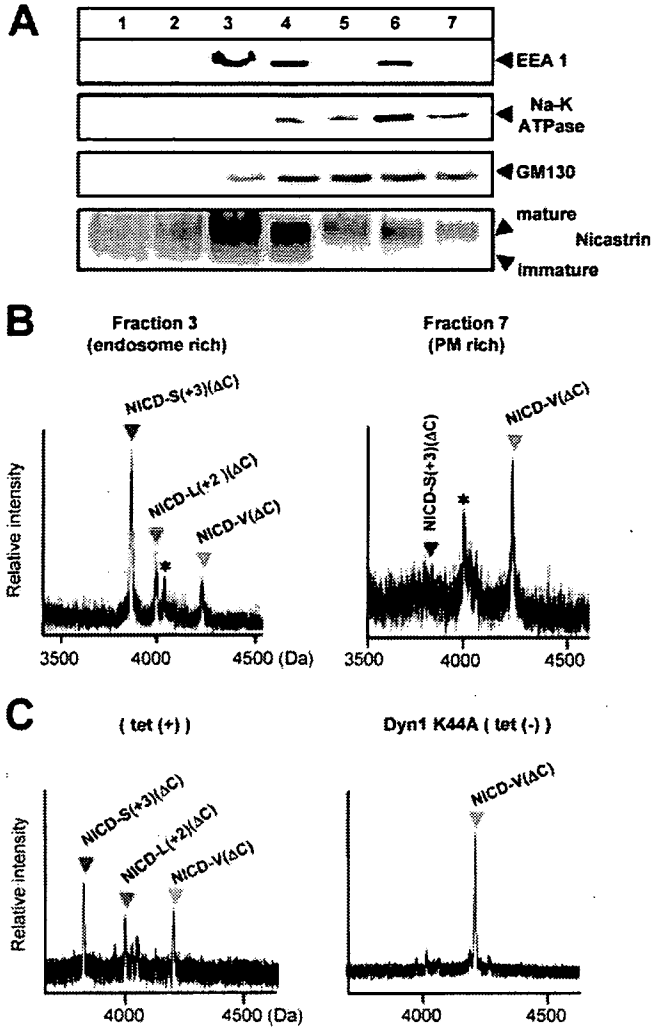

FIG. 6. Subcellular locations where S3-V and S3-S(+3) cleavages occur. (A) Fractions from a 2.5% to 25% linear iodixanol gradient examined by immunoblotting with the indicated antibodies. (B) MS spectra of NICD(ΔC) generated in the cell-free assay using membranes collected by centrifugation from the endosome-rich (fraction 3) and the PM-rich (fraction 7) fractions. Asterisks indicate nonspecific peaks. (C) MS spectra of NICD(ΔC) generated in the cell-free assay. CMFs from HeLa cells stably expressing NEXT(ΔC) and conditionally expressing Dyn-1 K44A were used. The precision of PS-dependent cleavage at the TM-cytoplasmic border in HeLa (left panel) and K293 (Fig. 1C) cells was different, in agreement with a previous report (11).

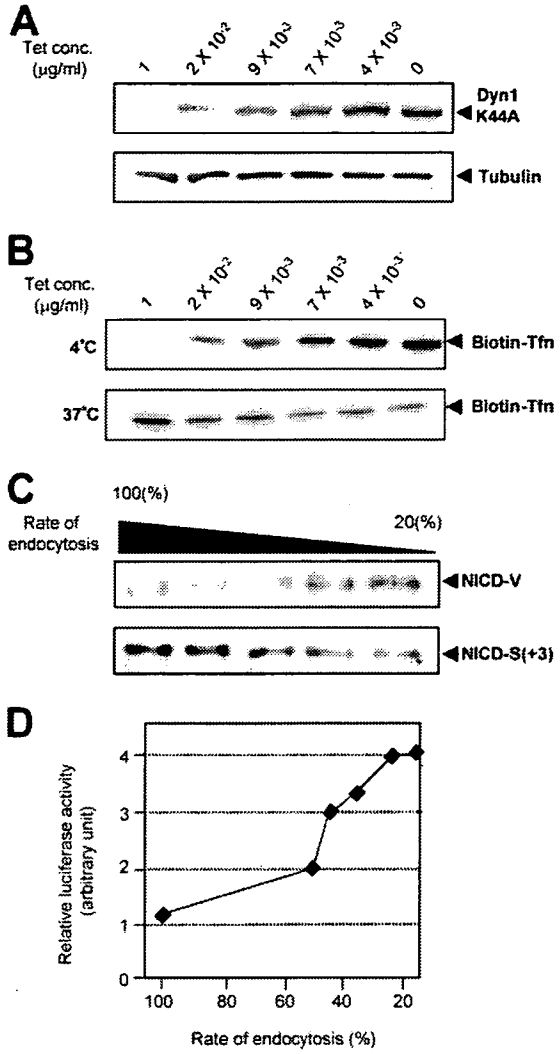

FIG. 7. Parallel change in the rate of endocytosis and the precision of S3 cleavage. (A) Expression of Dyn-1 K44A at various concentrations of tetracycline. Dyn-1 K44A/NEXT-coexpressing HeLa cells were cultured in medium with the indicated concentrations of tetracycline, and cell lysates were examined by immunoblotting with antibody 12CA5 (upper panel) or antitubulin (lower panel). The levels of Dyn-1 K44A increase as the concentration of tetracycline is decreased. (B) Various rates of endocytosis in Dyn-1 K44A expressing cells. Transferrin (Tfn) uptake assays were performed to measure the rate of endocytosis. The ratio of internalized Tfn (37°C; lower panel) to surface-bound Tfn (4°C; upper panel) in cells cultured in medium containing 1 μg/ml of tetracycline was defined as 100%. The rate of endocytosis decreased to ~15% when tetracycline was completely withdrawn. (C) Effect of the rate of endocytosis on the NICD species. The calculated rates of endocytosis were 100%, 41%, 37%, 21%, and 15% in lanes 1 to 5, respectively. (D) A plot of the relative Notch downstream luciferase activity versus the rate of endocytosis at various tetracycline concentrations.

mutant was found to be degraded mainly into NICD-L(+2)(ΔC), NICD-S(+3)(ΔC), and NICD-R(+5)(ΔC) species, which have unstable Leu1746, Ser1747, and the mutated Arg1749 at the N terminus, respectively (Fig. 8E). These results suggest that due to a dramatic change in the S3 cleavage precision, the Lys→Arg mutation causes not only a decrease of NICD-V but also an increase of extra unstable NICD species besides NICD-S(+3). This finding is reminiscent of the S3 cleavage for the Val→Gly mutant NEXT. Moreover, we studied whether NICDs in living cells expressing the Lys→Arg mutant are composed mainly of unstable NICD species. Strikingly, in the cells stably expressing the mutant NEXT, the stable NICD-V was barely detectable (13), while substantial amounts of NICDs were generated in the presence of the proteasome inhibitor mixture (Fig. 8F, top and middle panels). Since almost no NICD is observed in the mutant cells without the inhibitor mixture, it is indicated that NICDs in the Lys→Arg mutant-expressing cells are composed of unstable species (Fig. 8F, bottom panel). Therefore, the changes in the S3 cleavage precision induced by these S3 mutations are at

Downloaded from mcb.asm.org at Osaka University on March 12, 2008

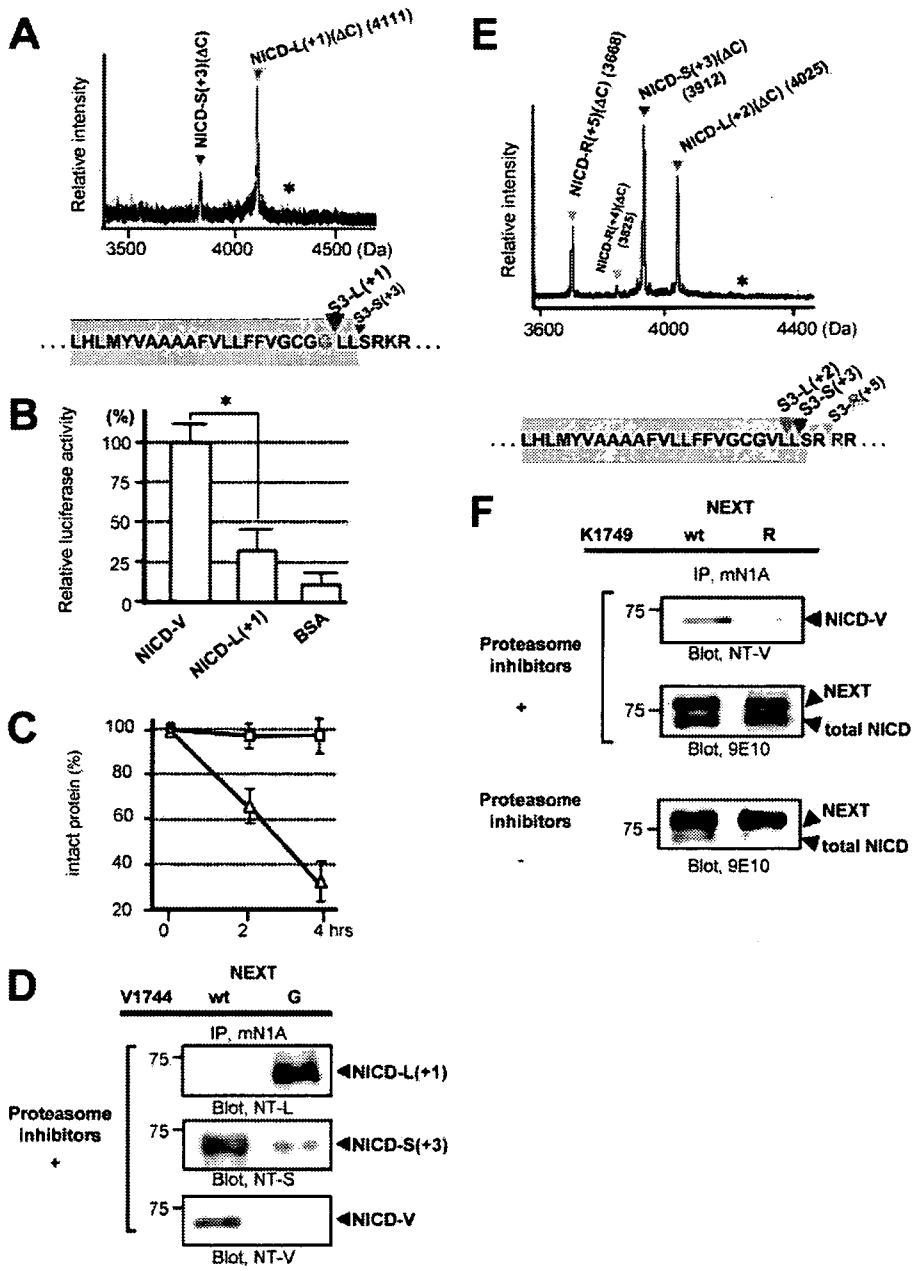

FIG. 8. Characteristics of the NICD species generated from the Val→Gly and the Lys→Arg mutants in cultured cells. (A) MS spectrum of de novo NICD(ΔC) generated from the Val→Gly mutant of NEXTΔC in K293 cells. The asterisk indicates the position of molecular mass corresponding to NICD-G(ΔC) species. Colored letters and inverted triangles show the mutation and proteolytic sites, respectively. (B) Assay of Notch downstream signaling induced by NICD-L(+1). Experiments were performed as described for Fig. 5B. The luciferase activity in the NICD-V-loaded cells was defined as 100%. Values represent means ± standard deviations. (n = 3). The asterisk indicates that the relative luciferase activity in NICD-V-loaded cells is statistically different than that in NICD-L(+1)-loaded cells ($P < 0.001$). (C) Degradation of NICD-L(+1) species in vitro. Experiments were performed as described for Fig. 5C but using NICD-L(+1) (triangles) and NICD-V (squares). Values represent means ± standard deviations (n = 3). (D) Generation of NICD-L(+1) and NICD-S(+3) in the Val→Gly mutant NEXT cells. K293 cells expressing either wt or the Val→Gly mutant NEXT were analyzed as described for Fig. 2D. (E) MS spectrum of de novo NICD(ΔC) generated from the Lys→Arg mutant of NEXTΔC in K293 cells. The asterisk indicates the position of molecular mass corresponding to NICD-V(ΔC) species. Colored letters and inverted triangles show the mutation and proteolytic sites, respectively. (F) Generation of unstable NICD species in the Lys→Arg mutant NEXT cells. K293 cells expressing either wt or the Lys→Arg mutant NEXT were analyzed as described for Fig. 2D (top and middle panels).

least partially responsible for the observed decrease in NICD level/Notch signaling in cultured cells.

Unlike several FAD-associated PS1 mutations, modifiers of PS/γ-secretase do not induce changes in the precision of S3 cleavage. Many FAD PS mutations affect the precision of not only γ but also ε cleavages of βAPP and, therefore, generally increase the relative AICDε48/AICDε49 ratio as well as the Aβ42/Aβ40 ratio (38, 42). In addition, compounds that modify the activity of PS/γ-secretase, including a subset of nonsteroidal anti-inflammatory drugs, cause reciprocal changes in rela-

Downloaded from mcb.asm.org at Osaka University on March 12, 2008

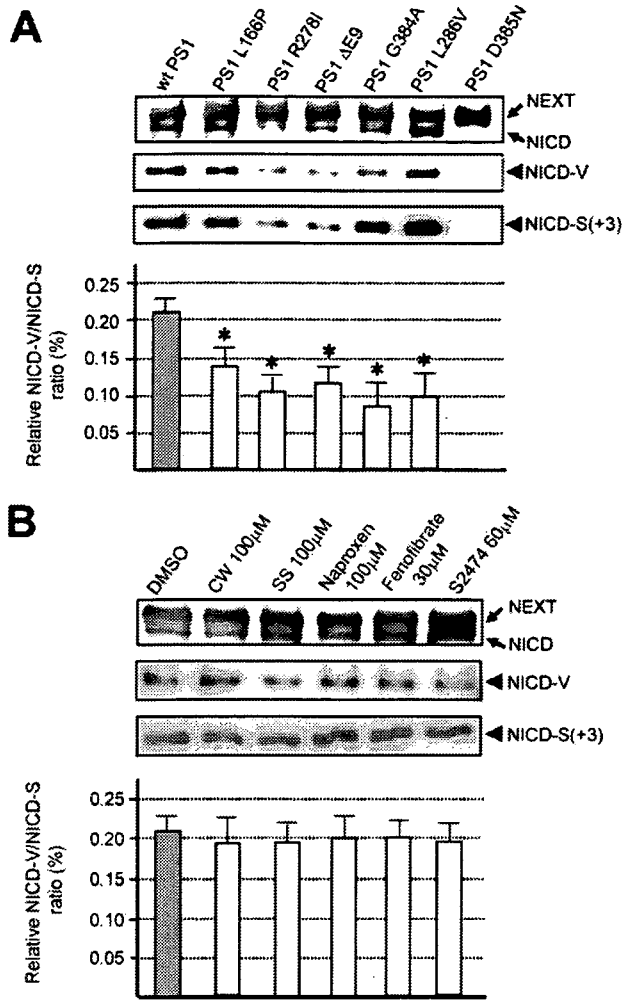

FIG. 9. Changes in the precision of S3 cleavage induced by FAD mutations in PS1. (A) Effect of several FAD PS1 mutations on the precision of S3 cleavage. K293 cells expressing the indicated PS mutant were transiently transfected with NEXT and analyzed as for Fig. 2D. The production of total NICD (first panel), NICD-V (second panel), and NICD-S(+3) (third panel) was assessed. Note that amount of total NICD was greatly reduced in PS1 R278I- and Δexon 9-expressing cells. The ratio of NICD-V to NICD-S(+3) in cells expressing wt PS1 or FAD mutants is shown in the bottom panel. Values represent means ± standard deviations (n = 3). The asterisk indicates that the ratio of NICD-V to NICD-S(+3) in cells expressing PS1 FAD mutants is significantly different from that in wt PS1-expressing cells ($P < 0.002$). (B) Effect of PS/γ-secretase modifiers on the precision of S3 cleavage. K293 cells stably expressing NEXT were treated with several PS/γ-secretase modifiers at the indicated concentration for 24 h and analyzed as described for the first three panels in panel A. DMSO, dimethyl sulfoxide; CW, compound W (31); SS, sulindac sulfide (49). The ratio of NICD-V to NICD-S(+3) in the control and treated cells is shown in the bottom panel. Values represent means ± standard deviations (n = 3).

tive production of Aβ42 and Aβ38 (19, 31, 49). Therefore, we investigated whether FAD PS mutations or PS/γ-secretase modifiers affect the precision of S3 cleavage. To evaluate the precision change, we used the relative NICD-V/NICD-S ratio, mimicking the relative Aβ42/Aβ40 ratio in the case of γ cleavage. Immunoblotting using anti-NT-V or anti-NT-S revealed that cells coexpressing PS1 mutants and NEXT produce both of the NICD species (Fig. 9A, top three panels). We found that the relative ratio of S3-V to S3-S(+3) cleavage was significantly reduced in some mutants (Fig. 9A, bottom panel). Subsequently, we examined the effects of PS/γ-secretase modifiers and naproxen (Fig. 9B). Because the effective doses of the compounds for γ and S3 cleavage may differ, we performed dose-response experiments to select the highest working concentrations (data not shown). After confirming that the level of Aβ42 in the medium was altered following a 24-h incubation with each compound (data not shown), we analyzed the cell lysates for the presence of NICD-V and NICD-S(+3) (Fig. 9B). In contrast to the case for the FAD mutants, the relative ratio of S3-V to S3-S(+3) cleavage was unchanged by the modifiers. These results suggest that γ-secretase modifiers do not affect the precision of intramembrane proteolysis by PS/γ-secretase.

DISCUSSION

The current studies suggest a novel mode by which the intensity of Notch signaling is regulated. We found that intracellular Notch signaling molecules (NICDs) in target cells can be divided into a stable one that transmits a substantial signal and unstable ones that transmit a much weaker signal, depending on the specific site of S3 cleavage. Therefore, Notch signaling intensity transmitted by conversion of extracellular signaling into intracellular signaling could depend on the characteristics of the target cell. For example, although S3 cleavage occurs, cells might not receive a substantial Notch signal when predominantly unstable NICDs are generated. On the basis of our results, we propose that the precision of S3 cleavage by PS/γ-secretase in the target cell is an important factor in determining the signaling intensity.

PS-dependent proteolysis on the TM of Notch-1 and βAPP consists of dual cleavage at the S4/S3 and γ/ε sites, respectively (14, 31, 33). The finding of diversity in the site of S3 cleavage means that cleavage at all four sites in the TM of Notch-1 and βAPP can vary. Thus, we suggest that the existence of variability in both the site and precision of cleavage may be a common feature of PS-dependent intramembrane proteolysis. Furthermore, we found that the precision of cleavage at S3 changes according to the subcellular location. On the PM, cleavage is more likely at S3-V, whereas on endosomes, cleavage is more likely at S3-S(+3), which is more C terminal. Interestingly, we have obtained very similar results regarding the cleavage of βAPP at the ε site (11). The precision of cleavage at the ε site changes depending on the subcellular location (11). The ε49 cleavage, which topologically corresponds to S3-V, occurs mainly on the PM, whereas the more C-terminal ε51 cleavage, which topologically corresponds to S3-S, occurs mainly on endosomes. Therefore, we have demonstrated that such subcellular location-dependent changes in the precision of the cleavage by PS/γ-secretase are common to the substrates. These findings suggest that such changes reflect a functional alteration of PS/γ-secretase in each subcellular location.

S2 cleavage upon ligand binding should occur on the PM of the target cells, but whether the subsequent S3 cleavage occurs on the PM or after endocytosis remains controversial (13, 17, 20, 46). The results of the current study suggest that (i) S3 cleavage occurs in both subcellular fractions in cell culture and

Downloaded from mcb.asm.org at Osaka University on March 12, 2008

(ii) S3-V cleavage, which generates stable NICD-V, occurs predominantly on the PM, whereas S3-S(+3) cleavage, which generates unstable NICD-S(+3), occurs predominantly on endosomes. We also found that the intensity of Notch signaling changes along with the extent of endocytosis, perhaps due to a change in the precision of S3 cleavage. Therefore, our results suggest that NICD generation on the PM and endosomes increases and decreases the intensity of Notch signaling, respectively. Reports that Sanpodo positively regulates Notch signaling on the PM and that Numb, a negative regulator, promotes endocytosis of Notch receptors and/or Sanpodo are consistent with our findings (3, 28). A previous study showed that *Drosophila* with a mutation in *shibire*, which encodes a homolog of dynamin, has a phenotype indicating a loss of Notch function (43). Further study to solve the contradiction is necessary.

Elimination of either Notch or PS function causes a strong Notch loss-of-function phenotype in vivo (23, 41). Knock-in mice with the S3 (Val→Gly) mutant of Notch-1 display a hypomorphic Notch phenotype, possibly due to reduced Notch signaling caused by a decrease in the intracellular NICD level (6, 15, 39). This reduction in the level of NICD polypeptides could be due to decreased generation and/or increased degradation (4, 6). Previously, NICD was considered to be a single polypeptide mediating a single type of signaling, implying that the lower level of NICD is due to a decrease in its generation; however, we found that the N termini of NICDs may play critical roles in their stabilities and thus signaling intensities.

Among S3 mutants of Notch-1, the Lys→Arg mutant NEXT is neither monoubiquitinated at Arg1749 nor endocytosed (13). Concurrently, the NICD-V level in the cells expressing this mutant is low (13). In this paper, we demonstrated that the Lys→Arg mutation also causes a drastic change in the precision of the S3 cleavage, which results in a drastic decrease of NICD-V generation on the PM. This explanation, if valid, resolves the discrepancy between the two studies.

Both stabilizing (Val, Met, or Gly) and destabilizing amino acid residues seem to be conserved in Notch orthologs of various organisms (see Table S2 in the supplemental material). This suggests that both stable and unstable intracellular Notch signaling exists in many species. Previous studies have indicated that differences in the intensity, duration, and timing of Notch signaling in target cells affect cell fate decisions (7, 26). Furthermore, the signaling by a molecule is dependent on its lifetime in the cell, and the lifetime should be short enough for the target cell to be able to rapidly change the extent of signaling (22). Therefore, target cells in different contexts may convert extracellular signals to various relative amounts of short- and long-term Notch signals.

FAD PS mutations generally increase the generation of Aβ42 (42). This pathological gain of function of PS is due to a change in the precision of γ cleavage, resulting in an increase in cleavage at γ42 (42). PS/γ-secretase modifiers can up- or down-regulate the cleavage at γ42 (19, 31, 49). In both cases, the modifiers have reciprocal effects on the production of Aβ42 and Aβ38 (31, 49). In this study, we found that several FAD PS1 mutants change the precision of S3 cleavage but that the PS/γ-secretase modifiers do not. These findings are consistent with previous studies showing that the precision of ε cleavage in βAPP is altered by certain FAD PS mutations (38) and that Notch processing is unaffected by nonsteroidal anti-inflammatory drugs that can reduce Aβ42 generation (45, 49). PS/γ-secretase modifiers could thus affect the precision of the intramembrane proteolysis differently from PS FAD mutations.

Because up-regulation in Notch signaling is involved in a subset of malignancies (10, 37, 47, 50), γ-secretase inhibitors have been considered for the treatment of cancer; however, inhibitors would cause the accumulation of substrates (i.e., NEXT), inevitably producing a "rebound effect," where the concentration of NICD would increase. Therefore, compounds that alter the precision of S3 cleavage and specifically inhibit the generation of stable NICD-V may be more effective therapeutic agents.

ACKNOWLEDGMENTS

We thank J. Takeda, R. Kopan, M. Nishimura, H. Hasegawa, Y. Eguchi, Y. Tsujimoto, H. Steiner, and C. Haass for critically reading the manuscript and S. Shirahata, R. Kopan, J. S. Nye, A. Israel, S. L. Schmid, and G. W. Bornkamm for providing cDNAs, constructs, and cell lines.

M.O. conceived and designed the experiments. S.T. and others performed the experiments. M.O. wrote the paper.

We are grateful for funding from the Program for the Promotion of Fundamental Studies in Health Sciences of the National Institute of Biomedical Innovation (05-26) (to M.T., M.O., and S.T.), grants-in-aid for Scientific Research on Priority Areas-Advanced Brain Science Project (to M.O.) and KAKEN-HI from the Ministry of Education, Culture, Sports, Science, and Technology (to M.T., M.O., and S.T.), and grants-in-aid from the Japanese Ministry of Health, Labor and Welfare (to M.T. and M.O.).

We declare that no competing interests exist.

REFERENCES

1. **Artavanis-Tsakonas, S., M. D. Rand, and R. J. Lake.** 1999. Notch signaling: cell fate control and signal integration in development. Science **284**:770–776.
2. **Bachmair, A., D. Finley, and A. Varshavsky.** 1986. In vivo half-life of a protein is a function of its amino-terminal residue. Science **234**:179–186.
3. **Berdnik, D., T. Torok, M. Gonzalez-Gaitan, and J. A. Knoblich.** 2002. The endocytic protein alpha-adaptin is required for numb-mediated asymmetric cell division in Drosophila. Dev. Cell **3**:221–231.
4. **Blat, Y., J. E. Meredith, Q. Wang, J. D. Bradley, L. A. Thompson, R. E. Olson, A. M. Stern, and D. Seiffert.** 2002. Mutations at the P1′ position of Notch1 decrease intracellular domain stability rather than cleavage by gamma-secretase. Biochem. Biophys. Res. Commun. **299**:569–573.
5. **Cao, X., and T. C. Sudhof.** 2001. A transcriptionally active complex of APP with Fe65 and histone acetyltransferase Tip60. Science **293**:115–120.
6. **Chandu, D., S. S. Huppert, and R. Kopan.** 2006. Analysis of transmembrane domain mutants is consistent with sequential cleavage of Notch by gamma-secretase. J. Neurochem. **96**:228–235.
7. Reference deleted.
8. **De Strooper, B., W. Annaert, P. Cupers, P. Saftig, K. Craessaerts, J. S. Mumm, E. H. Schroeter, V. Schrijvers, M. S. Wolfe, W. J. Ray, A. Goate, and R. Kopan.** 1999. A presenilin-1-dependent gamma-secretase-like protease mediates release of Notch intracellular domain. Nature **398**:518–522.
9. **Fehon, R. G., K. Johansen, I. Rebay, and S. Artavanis-Tsakonas.** 1991. Complex cellular and subcellular regulation of notch expression during embryonic and imaginal development of Drosophila: implications for notch function. J. Cell Biol. **113**:657–669.
10. **Fre, S., M. Huyghe, P. Mourikis, S. Robine, D. Louvard, and S. Artavanis-Tsakonas.** 2005. Notch signals control the fate of immature progenitor cells in the intestine. Nature **435**:964–968.
11. **Fukumori, A., M. Okochi, S. Tagami, J. Jiang, N. Itoh, T. Nakayama, K. Yanagida, Y. Ishizuka-Katsura, T. Morihara, K. Kamino, T. Tanaka, T. Kudo, H. Tanii, A. Ikuta, C. Haass, and M. Takeda.** 2006. Presenilin-dependent gamma-secretase on plasma membrane and endosomes is functionally distinct. Biochemistry **45**:4907–4914.
12. **Gonda, D. K., A. Bachmair, I. Wunning, J. W. Tobias, W. S. Lane, and A. Varshavsky.** 1989. Universality and structure of the N-end rule. J. Biol. Chem. **264**:16700–16712.
13. **Gupta-Rossi, N., E. Six, O. LeBail, F. Logeat, P. Chastagner, A. Olry, A. Israel, and C. Brou.** 2004. Monoubiquitination and endocytosis direct gamma-secretase cleavage of activated Notch receptor. J. Cell Biol. **166**:73–83.

Downloaded from mcb.asm.org at Osaka University on March 12, 2008

14. **Haass, C., and H. Steiner.** 2002. Alzheimer disease gamma-secretase: a complex story of GxGD-type presenilin proteases. Trends Cell Biol. **12**:556–562.
15. **Huppert, S. S., A. Le, E. H. Schroeter, J. S. Mumm, M. T. Saxena, L. A. Milner, and R. Kopan.** 2000. Embryonic lethality in mice homozygous for a processing-deficient allele of Notch1. Nature **405**:966–970.
16. **Jarriault, S., C. Brou, F. Logeat, E. H. Schroeter, R. Kopan, and A. Israel.** 1995. Signalling downstream of activated mammalian Notch. Nature **377**: 355–358.
17. **Kaether, C., S. Schmitt, M. Willem, and C. Haass.** 2006. Amyloid precursor protein and Notch intracellular domains are generated after transport of their precursors to the cell surface. Traffic **7**:408–415.
18. **Koo, E. H., and R. Kopan.** 2004. Potential role of presenilin-regulated signaling pathways in sporadic neurodegeneration. Nat. Med. **10**(Suppl.):S26–S33.
19. **Kukar, T., M. P. Murphy, J. L. Eriksen, S. A. Sagi, S. Weggen, T. E. Smith, T. Ladd, M. A. Khan, R. Kache, J. Beard, M. Dodson, S. Merit, V. V. Ozols, P. Z. Anastasiadis, P. Das, A. Fauq, E. H. Koo, and T. E. Golde.** 2005. Diverse compounds mimic Alzheimer disease-causing mutations by augmenting Abeta42 production. Nat. Med. **11**:545–550.
20. **Lopez-Schier, H., and D. St. Johnston.** 2002. Drosophila nicastrin is essential for the intramembranous cleavage of notch. Dev. Cell **2**:79–89.
21. **Minoguchi, S., Y. Taniguchi, H. Kato, T. Okazaki, L. J. Strobl, U. Zimber-Strobl, G. W. Bornkamm, and T. Honjo.** 1997. RBP-L, a transcription factor related to RBP-Jκ. Mol. Cell. Biol. **17**:2679–2687.
22. **Morimoto, M., Y. Takahashi, M. Endo, and Y. Saga.** 2005. The Mesp2 transcription factor establishes segmental borders by suppressing Notch activity. Nature **435**:354–359.
23. **Mumm, J. S., and R. Kopan.** 2000. Notch signaling: from the outside in. Dev. Biol. **228**:151–165.
24. **Mumm, J. S., E. H. Schroeter, M. T. Saxena, A. Griesemer, X. Tian, D. J. Pan, W. J. Ray, and R. Kopan.** 2000. A ligand-induced extracellular cleavage regulates gamma-secretase-like proteolytic activation of Notch1. Mol. Cell **5**:197–206.
25. **Munter, L. M., P. Voigt, A. Harmeier, D. Kaden, K. E. Gottschalk, C. Weise, R. Pipkorn, M. Schaefer, D. Langosch, and G. Multhaup.** 2007. GxxxG motifs within the amyloid precursor protein transmembrane sequence are critical for the etiology of Abeta42. EMBO J. **26**:1702–1712.
26. **Nakagawa, M., M. Ichikawa, K. Kumano, S. Goyama, M. Kawazu, T. Asai, S. Ogawa, M. Kurokawa, and S. Chiba.** 2006. AML1/Runx1 rescues Notch1-Null mutation-induced deficiency of para-aortic splanchnopleural hematopoiesis. Blood **108**:3329–3334.
27. **Nakaya, Y., T. Yamane, H. Shiraishi, H. Q. Wang, E. Matsubara, T. Sato, G. Dolios, R. Wang, B. De Strooper, M. Shoji, H. Komano, K. Yanagisawa, Y. Ihara, P. Fraser, P. St George-Hyslop, and M. Nishimura.** 2005. Random mutagenesis of presenilin-1 identifies novel mutants exclusively generating long amyloid beta-peptides. J. Biol. Chem. **280**:19070–19077.
28. **O'Connor-Giles, K. M., and J. B. Skeath.** 2003. Numb inhibits membrane localization of Sanpodo, a four-pass transmembrane protein, to promote asymmetric divisions in Drosophila. Dev. Cell **5**:231–243.
29. **Ohashi, H., and T. Sudo.** 1994. Efficient expression of a transfected foreign gene by Cos1 cells in serum-free medium. Biosci. Biotechnol. Biochem. **58**:758–759.
30. **Okochi, M., S. Eimer, A. Bottcher, R. Baumeister, H. Romig, J. Walter, A. Capell, H. Steiner, and C. Haass.** 2000. A loss of function mutant of the presenilin homologue SEL-12 undergoes aberrant endoproteolysis in Caenorhabditis elegans and increases abeta 42 generation in human cells. J. Biol. Chem. **275**:40925–40932.
31. **Okochi, M., A. Fukumori, J. Jiang, N. Itoh, R. Kimura, H. Steiner, C. Haass, S. Tagami, and M. Takeda.** 2006. Secretion of the Notch-1 Abeta-like peptide during Notch signaling. J. Biol. Chem. **281**:7890–7898.
32. **Okochi, M., K. Ishii, M. Usami, N. Sahara, F. Kametani, K. Tanaka, P. E. Fraser, M. Ikeda, A. M. Saunders, L. Hendriks, S. I. Shoji, L. E. Nee, J. J. Martin, C. Van Broeckhoven, P. H. St George-Hyslop, A. D. Roses, and H. Mori.** 1997. Proteolytic processing of presenilin-1 (PS-1) is not associated with Alzheimer's disease with or without PS-1 mutations. FEBS Lett. **418**: 162–166.
33. **Okochi, M., H. Steiner, A. Fukumori, H. Tanii, T. Tomita, T. Tanaka, T. Iwatsubo, T. Kudo, M. Takeda, and C. Haass.** 2002. Presenilins mediate a dual intramembranous gamma-secretase cleavage of Notch-1. EMBO J. **21**: 5408–5416.
34. **Okochi, M., J. Walter, A. Koyama, S. Nakajo, M. Baba, T. Iwatsubo, L. Meijer, P. J. Kahle, and C. Haass.** 2000. Constitutive phosphorylation of the Parkinson's disease associated alpha-synuclein. J. Biol. Chem. **275**:390–397.
35. **Parks, A. L., K. M. Klueg, J. R. Stout, and M. A. Muskavitch.** 2000. Ligand endocytosis drives receptor dissociation and activation in the Notch pathway. Development **127**:1373–1385.
36. **Qi-Takahara, Y., M. Morishima-Kawashima, Y. Tanimura, G. Dolios, N. Hirotani, Y. Horikoshi, F. Kametani, M. Maeda, T. C. Saido, R. Wang, and Y. Ihara.** 2005. Longer forms of amyloid beta protein: implications for the mechanism of intramembrane cleavage by gamma-secretase. J. Neurosci. **25**:436–445.
37. **Radtke, F., and K. Raj.** 2003. The role of Notch in tumorigenesis: oncogene or tumour suppressor? Nat. Rev. Cancer **3**:756–767.
38. **Sato, T., N. Dohmae, Y. Qi, N. Kakuda, H. Misonou, R. Mitsumori, H. Maruyama, E. H. Koo, C. Haass, K. Takio, M. Morishima-Kawashima, S. Ishiura, and Y. Ihara.** 2003. Potential link between amyloid beta-protein 42 and C-terminal fragment gamma 49–99 of beta-amyloid precursor protein. J. Biol. Chem. **278**:24294–24301.
39. **Schroeter, E. H., J. A. Kisslinger, and R. Kopan.** 1998. Notch-1 signalling requires ligand-induced proteolytic release of intracellular domain. Nature **393**:382–386.
40. **Schweisguth, F.** 2004. Notch signaling activity. Curr. Biol. **14**:R129–R138.
41. **Selkoe, D., and R. Kopan.** 2003. Notch and Presenilin: regulated intramembrane proteolysis links development and degeneration. Annu. Rev. Neurosci. **26**:565–597.
42. **Selkoe, D. J.** 2001. Alzheimer's disease: genes, proteins, and therapy. Physiol. Rev. **81**:741–766.
43. **Seugnet, L., P. Simpson, and M. Haenlin.** 1997. Requirement for dynamin during Notch signaling in Drosophila neurogenesis. Dev. Biol. **192**:585–598.
44. **Steiner, H., M. Kostka, H. Romig, G. Basset, B. Pesold, J. Hardy, A. Capell, L. Meyn, M. L. Grim, R. Baumeister, K. Fechteler, and C. Haass.** 2000. Glycine 384 is required for presenilin-1 function and is conserved in bacterial polytopic aspartyl proteases. Nat. Cell Biol. **2**:848–851.
45. **Takahashi, Y., I. Hayashi, Y. Tominari, K. Rikimaru, Y. Morohashi, T. Kan, H. Natsugari, T. Fukuyama, T. Tomita, and T. Iwatsubo.** 2003. Sulindac sulfide is a noncompetitive gamma-secretase inhibitor that preferentially reduces Abeta 42 generation. J. Biol. Chem. **278**:18664–18670.
46. **Tarassishin, L., Y. I. Yin, B. Bassit, and Y. M. Li.** 2004. Processing of Notch and amyloid precursor protein by gamma-secretase is spatially distinct. Proc. Natl. Acad. Sci. USA **101**:17050–17055.
47. **van Es, J. H., M. E. van Gijn, O. Riccio, M. van den Born, M. Vooijs, H. Begthel, M. Cozijnsen, S. Robine, D. J. Winton, F. Radtke, and H. Clevers.** 2005. Notch/gamma-secretase inhibition turns proliferative cells in intestinal crypts and adenomas into goblet cells. Nature **435**:959–963.
48. **Washburn, T., E. Schweighoffer, T. Gridley, D. Chang, B. J. Fowlkes, D. Cado, and E. Robey.** 1997. Notch activity influences the alphabeta versus gammadelta T cell lineage decision. Cell **88**:833–843.
49. **Weggen, S., J. L. Eriksen, P. Das, S. A. Sagi, R. Wang, C. U. Pietrzik, K. A. Findlay, T. E. Smith, M. P. Murphy, T. Bulter, D. E. Kang, N. Marquez-Sterling, T. E. Golde, and E. H. Koo.** 2001. A subset of NSAIDs lower amyloidogenic Abeta42 independently of cyclooxygenase activity. Nature **414**:212–216.
50. **Weng, A. P., A. A. Ferrando, W. Lee, J. P. t. Morris, L. B. Silverman, C. Sanchez-Irizarry, S. C. Blacklow, A. T. Look, and J. C. Aster.** 2004. Activating mutations of NOTCH1 in human T cell acute lymphoblastic leukemia. Science **306**:269–271.
51. **Wolfe, M. S., W. Xia, B. L. Ostaszewski, T. S. Diehl, W. T. Kimberly, and D. J. Selkoe.** 1999. Two transmembrane aspartates in presenilin-1 required for presenilin endoproteolysis and gamma-secretase activity. Nature **398**: 513–517.
52. **Xia, W., and M. S. Wolfe.** 2003. Intramembrane proteolysis by presenilin and presenilin-like proteases. J. Cell Sci. **116**:2839–2844.
53. **Zhao, G., M. Z. Cui, G. Mao, Y. Dong, J. Tan, L. Sun, and X. Xu.** 2005. Gamma-cleavage is dependent on zeta-cleavage during the proteolytic processing of amyloid precursor protein within its transmembrane domain. J. Biol. Chem. **280**:37689–37697.

Downloaded from mcb.asm.org at Osaka University on March 12, 2008

Molecular Psychiatry (2007), 1–7
© 2007 Nature Publishing Group All rights reserved 1359-4184/07 $30.00
www.nature.com/mp

ORIGINAL ARTICLE

Pituitary adenylate cyclase-activating polypeptide is associated with schizophrenia

R Hashimoto[1,2,3,11], H Hashimoto[1,4,11], N Shintani[4,11], S Chiba[2,3], S Hattori[3], T Okada[3], M Nakajima[4], K Tanaka[4], N Kawagishi[4], K Nemoto[5], T Mori[3,5], T Ohnishi[3,5], H Noguchi[3], H Hori[3], T Suzuki[6], N Iwata[6], N Ozaki[7], T Nakabayashi[8], O Saitoh[8], A Kosuga[9], M Tatsumi[9], K Kamijima[9], DR Weinberger[10], H Kunugi[3] and A Baba[4]

[1]*The Osaka-Hamamatsu Joint Research Center for Child Mental Development, Osaka University Graduate School of Medicine, Suita, Osaka, Japan;* [2]*Department of Psychiatry, Osaka University Graduate School of Medicine, Suita, Osaka, Japan;* [3]*Department of Mental Disorder Research, National Institute of Neuroscience, National Center of Neurology and Psychiatry, Kodaira, Tokyo, Japan;* [4]*Laboratory of Molecular Neuropharmacology, Graduate School of Pharmaceutical Sciences, Osaka University, Suita, Osaka, Japan;* [5]*Department of Radiology, National Center Hospital of Mental, Nervous, and Muscular Disorders, National Center of Neurology and Psychiatry, Kodaira, Tokyo, Japan;* [6]*Department of Psychiatry, Fujita Health University School of Medicine, Toyoake, Aichi, Japan;* [7]*Department of Psychiatry, Nagoya University Graduate School of Medicine, Nagoya, Aichi, Japan;* [8]*Department of Psychiatry, National Center Hospital of Mental, Nervous, and Muscular Disorders, National Center of Neurology and Psychiatry, Kodaira, Tokyo, Japan;* [9]*Department of Psychiatry, Showa University School of Medicine, Shinagawaku, Tokyo, Japan and* [10]*Genes, Cognition, and Psychosis Program, Clinical Brain Disorders Branch, National Institute of Mental Health, National Institutes of Health, Bethesda, MD, USA*

Pituitary adenylate cyclase-activating polypeptide (PACAP, ADCYAP1: adenylate cyclase-activating polypeptide 1), a neuropeptide with neurotransmission modulating activity, is a promising schizophrenia candidate gene. Here, we provide evidence that genetic variants of the genes encoding PACAP and its receptor, PAC1, are associated with schizophrenia. We studied the effects of the associated polymorphism in the PACAP gene on neurobiological traits related to risk for schizophrenia. This allele of the PACAP gene, which is overrepresented in schizophrenia patients, was associated with reduced hippocampal volume and poorer memory performance. Abnormal behaviors in PACAP knockout mice, including elevated locomotor activity and deficits in prepulse inhibition of the startle response, were reversed by treatment with an atypical antipsychotic, risperidone. These convergent data suggest that alterations in PACAP signaling might contribute to the pathogenesis of schizophrenia.
Molecular Psychiatry advance online publication, 27 March 2007; doi:10.1038/sj.mp.4001982

Keywords: schizophrenia; PACAP; SNP; hippocampus; memory; PPI

Introduction

Schizophrenia is a common neuropsychiatric disorder affecting 0.5–1% of the general population worldwide. This disease is characterized by psychosis and profound disturbances of cognition, emotion and social functioning. The pathophysiology of schizophrenia is still unclear; however, this disease is highly heritable[1] and several intermediate phenotypes such as neurocognitive dysfunction, abnormal brain morphology and deficits in prepulse inhibition (PPI) of the startle response are known to be useful to identify susceptibility genes for schizophrenia.[2,3]

Correspondence: Dr R Hashimoto, The Osaka-Hamamatsu Joint Research Center for Child Mental Development, Osaka University Graduate School of Medicine, D3, 2-2, Yamadaoka, Suita, Osaka, 565-0871, Japan.
E-mail: hashimor@psy.med.osaka-u.ac.jp
[11]These authors contributed equally to this work.
Received 2 October 2006; revised 17 January 2007; accepted 20 February 2007

The adenylate cyclase-activating polypeptide 1 (ADCYAP1) gene encodes pituitary adenylate cyclase-activating polypeptide (PACAP), a neuropeptide, which is a member of the vasoactive intestinal peptide (VIP)/secretin/glucagon family. It exerts multiple activities as a neurotransmitter or neuromodulator via three heptahelical G-protein-linked receptors, one PACAP-specific (PAC1) receptor and two receptors that are shared with VIP (VPAC1 and VPAC2).[4–6] PACAP induces cyclic AMP accumulation through activation of these receptors.[4–6] We generated mice lacking the PACAP gene ($PACAP^{-/-}$); these mice had profound behavioral abnormalities including hyperactivity and explosive jumping in an open field, increased novelty-seeking behavior and deficits in PPI.[7,8] In addition, the PACAP gene is located on 18p11, which linkage studies have suggested as a locus for schizophrenia and bipolar disorder.[9] Although previous studies indicated that the PACAP gene could be a good candidate gene for schizophrenia, only one preliminary study has examined a

possible association with schizophrenia and reported negative results.[10] Here, we present data demonstrating a possible association between PACAP-PAC1 signaling and schizophrenia, using a multidisciplinary approach in both humans and rodents.

Materials and methods

Subjects

Subjects for the clinical association study were 804 patients with schizophrenia (51.1% males with a mean age of 44.2 years (s.d. 14.5) and a mean age of onset of 24.8 years (s.d. 8.8)) and 967 healthy controls (47.7% males with a mean age of 40.4 years (s.d. 16.1)). All the subjects were biologically unrelated Japanese. Three hundred and fifty-one patients with schizophrenia and 518 controls were from Tokyo Metropolitan (the east part of Japan), and 453 patients with schizophrenia and 449 controls were from Aichi prefecture (the central part of Japan). Patients were recruited at the National Center Hospital of Mental, Nervous, and Muscular Disorders; Nagoya University Hospital; Showa University Hospital and hospitals related to Department of Psychiatry, Nagoya University Graduate School of Medicine or Department of Psychiatry, Showa University School of Medicine. Healthy controls, including hospital and institutional staff, were recruited from local advertisements in Tokyo and Aichi. Magnetic resonance (MR) measurements and neurocognitive tests were performed only on some subjects (MR measurements: 81 patients with schizophrenia and 201 healthy controls; neurocognitive tests: 62 patients with schizophrenia and 139 healthy controls), all of whom were recruited at National Center of Neurology and Psychiatry. Demographic information for the subjects receiving MR measurements and neurocognitive tests is shown in detail in Supplementary Table 1 and Figure 1b. Consensus diagnosis was made for each patient by at least two trained psychiatrists, according to the Diagnostic and Statistical Manual of Mental Disorders, fourth edition (DSM-IV) criteria, based on clinical interview and other available information including medical records and other research assessments. No patient was diagnosed by medical records alone. Controls were healthy volunteers who had no current or past contact to psychiatric services. After a description of the study, written informed consent was obtained from every subject. The study protocol was approved by institutional ethics committees.

Genetic analysis

Venous blood was drawn from subjects and genomic DNA was extracted from whole blood according to standard procedures. Seven single nucleotide polymorphisms (SNPs) in the PACAP gene and three SNPs in the PAC1, VPAC1 and VPAC2 genes were genotyped using the TaqMan 5′-exonuclease allelic discrimination assay, as described previously.[11,12] Primers and probes for the detection of the SNPs are available on request. Statistical analysis of genetic association studies was performed using SNPAlyse (DYNACOM, Yokohama, Japan). The presence of Hardy–Weinberg equilibrium was examined by using the χ^2 test for goodness of fit. Allele distributions between patients and controls were analyzed by the χ^2 test for independence. All *P*-values reported are two-tailed. Statistical significance was defined as $P < 0.05$.

Neuroimaging analysis

All MR studies were performed on a 1.5 T Siemens Magnetom Vision plus system (Siemens, Erlangen, Germany). A three-dimensional volumetric acquisition of a T1-weighted gradient echo sequence produced a gapless series of 144 sagittal sections using an MPRage sequence (TE/TR, 4.4/11.4 ms; flip angle, 15°; acquisition matrix, 256 × 256; 1NEX, field of view, 31.5 cm; slice thickness, 1.23 mm).

Data were analyzed with Statistical Parametric Mapping 2 (SPM2) running on MATLAB 6.5. MR images were processed using optimized voxel-based morphometry (VBM) in SPM2 as described in detail previously.[13,14] Normalized segmented images were modulated by multiplication with Jacobian determinants of the spatial normalization to encode the deformation field for each subject as tissue density changes in normal space. Following modulation, images were smoothed using a 12 mm full-width half-maximum of isotropic Gaussian kernel, because previous studies had proved that this should be a reasonable filter.[13,15,16] In addition, we confirmed that the results of statistical analyses with three different smoothing filters (6, 8 and 12 mm Gaussian kernels) were essentially the same.

Statistical analyses were performed with SPM2, which implemented a general linear model. A hypothesis-driven regions of interest (ROIs) approach was used to investigate the hippocampus, using an ROI from the Wake Forest University PickAtlas.[17] Our hypothesis is that the PACAP genotype related to the risk of developing schizophrenia is associated with hippocampal volume, because PACAP is associated with hippocampal function in rodents, and hippocampal volume is reported to be reduced in schizophrenia. The genotype and diagnostic effects on hippocampal gray matter volume change were assessed statistically using a single-subject condition and covariate model with a significance level set to 0.05 (corrected for multiple comparisons within the ROI). Age and gender were included in the model to control for confounds. Anatomic localization was according to both MNI coordinates and Talairach coordinates, obtained from M. Brett's transformations (http://www.mrccbu.cam.ac.uk/Imaging/Common/mnispace.shtml) and presented as Talairach coordinates.

Neurocognitive tests

Several memory tests, subscales of the Wechsler Memory Scale revised version (logical memory I, logical memory II, visual reproduction I, visual reproduction II, verbal paired associates I (VPAI),

verbal paired associates II, visual paired associates I and visual paired associates II) and the general intelligence IQ (from full scale of the Wechsler Adult Intelligence Scale, revised edition, WAIS-R), were performed by some of the subjects recruited at National Center of Neurology and Psychiatry. In association analysis between SNP3 of the PACAP gene and VPAI, group comparisons of demographic data were performed by using unpaired *t*-tests or χ^2, as appropriate. There were no differences between genotype groups and demographic variables, for example, age, gender, education years and full-scale IQ, except for gender distribution in patients with schizophrenia ($P=0.026$) (Figure 1b). The effects of the SNP3 genotype of the PACAP gene and diagnosis on scores of memory tests were analyzed by a two-way analysis of covariance (ANCOVA), with age, gender and education years as covariates using SPSS 11.0J for Windows (SPSS Japan Inc., Tokyo, Japan).

a

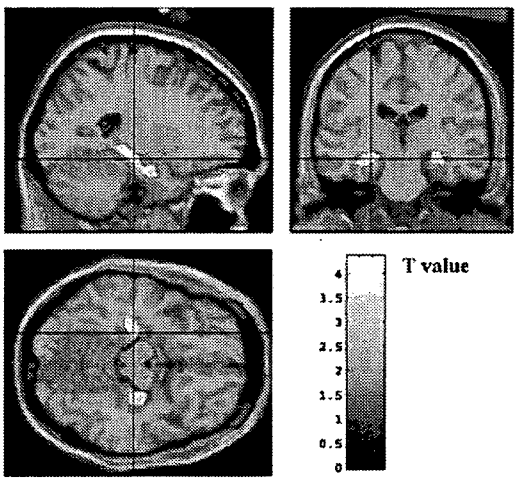

b

	Schizophrenia (n=62)		Control (n=139)	
Variables	A/A, A/G (n=10)	G/G (n=52)	A/A, A/G (n=27)	G/G (n=112)
Age (SD)	39.2 (10.5)	47.1 (13.7)	34.6 (11.0)	37.3 (11.8)
Gender (M/F)	3/7	35/17	13/14	34/78
Education years (SD)	14.0 (2.6)	12.8 (3.3)	16.7 (2.8)	16.5 (3.1)
Full scale IQ (SD)	86.2 (21.5)	83.8 (18.8)	109.9 (13.4)	109.6 (11.6)
VPA1 (SD)	13.3 (3.9)	9.0 (4.6)*	16.1 (2.7)	16.1 (2.3)

Figure 1 Genetic variation of PACAP is associated with hippocampal morphology and memory in humans. (**a**) Statistical maps of *t*-transformed hippocampal volume differences derived by optimized VBM of individuals homozygous for the G allele in SNP3 of the PACAP gene, relative to A-carriers, in all subjects, thresholded at $P<0.05$ (corrected) in coronal, sagittal and axial views. These data show bilateral significant hippocampal volume reduction in individuals homozygous for the G allele. (**b**) Lower visual associate memory I score in individuals homozygous for the G allele in SNP3 of the PACAP gene, compared to A-carriers, in the schizophrenia group. Means ± s.d. are shown. VPAI, visual paired associates I. $^*P<0.05$, compared with A-carriers.

When genotype effects on VPAI in controls or patients with schizophrenia were examined separately, a Mann–Whitney *U*-test and ANCOVA with gender as a covariate were used.

Animal study

All animal experiments were carried out in accordance with protocols approved by the Animal Research Committee of Osaka University and by the Ethics Review Committee for Animal Experimentation of the National Institute of Neuroscience. Generation of PACAP$^{-/-}$ mice by a gene targeting technique has been reported previously.[7] The null mutation was backcrossed onto the genetic background of Crlj:CD1 (Institute of Cancer Research) mice purchased from Charles River (Tokyo, Japan). All wild-type control mice and PACAP$^{-/-}$ mice (homozygous for the mutant PACAP gene) used in locomotor activity and PPI experiments were obtained from the intercross of heterozygous animals. C57BL/6J mice were purchased from Charles River and were allowed to acclimate in our animal facility for at least 5 days before initiation of experiments. Mice were housed in a temperature- (23 ± 1°C) and light-controlled room with a 12 h light–dark cycle (lights on from 0800 to 2000) and allowed free access to water and food, except during behavioral testing.

Locomotor activity was quantified using an infrared photocell beam detection system, Acti-Track (Panlab, Barcelona, Spain). Following intraperitoneal injection of risperidone (0.1 mg/kg) or an equivalent amount of saline, mice were placed in plastic activity monitoring boxes ($30\times30\times30$ cm) and tracked for 60 min, with data being stored permanently; parameters indicative of locomotor activity, such as distance traveled, were assessed. Each mouse was tested individually and had no contact with the other mice. The PACAP mutant cohort used in locomotor activity testing consisted of 12 wild-type mice and 12 PACAP$^{-/-}$ mice ($n=6$ each for saline control and risperidone groups).

Acoustic startle responses for PPI were measured in a startle chamber (SR-LAB; San Diego Instruments, CA, USA) as described.[18] Mice were placed in the startle chamber for 30 min after intraperitoneal injection of risperidone (0.1 mg/kg) or an equal amount of saline. The testing session started with 5 min of acclimatization to the startle chamber in the presence of 65 dB background broadband (white) noise. Testing consisted of forty 120 dB pulses alone and 10 pulses preceded (100 ms) by a prepulse of 66, 68, 71 or 77 dB. Pulses were randomly presented with an average of 15 s between pulses. Twelve no-stimulus trials were included to assess spontaneous activity during testing. PPI was calculated as a percentage score: PPI (%) = (1−((startle response for pulse with prepulse)/(startle response for pulse alone))) × 100. The PACAP mutant cohort used in PPI testing consisted of 35 wild-type mice (saline control group = 22; risperidone group = 13) and 33 PACAP$^{-/-}$ mice (saline control group = 17; risperidone group = 16).

Male C57BL/6J mice weighing 20–25 g received once-daily injections intraperitoneally for 14 days with phencyclidine (PCP) (5 mg/kg; $n=13$) or saline for control ($n=12$). PACAP and PAC1 mRNA levels were measured by a real-time quantitative RT–PCR method (TaqMan assay, Applied Biosystems, Tokyo, Japan), using total RNA extracted from the frontal cortex or hippocampus of mice treated with PCP or saline, as described previously.[19] Statistically significant differences were assessed by the Mann–Whitney *U*-test.

Results

Genetic analysis

We examined the possible association between schizophrenia and genetic variations in the PACAP gene. Seven SNPs in the PACAP gene, selected from public databases, were genotyped, and the genotype distributions of all seven SNPs in the PACAP gene were in Hardy–Weinberg equilibrium in both controls and patients with schizophrenia (data not shown). The allele frequencies of the seven SNPs in patients and controls are shown in Table 1. The major allele of SNP3 and the minor allele of SNP5 were in excess in patients with schizophrenia when compared to controls (SNP3: $\chi^2=7.6$, $P=0.0059$, odds ratio = 0.74, 95% confidence interval (CI) 0.59–0.92; SNP5: $\chi^2=4.2$, $P=0.041$, odds ratio = 1.38, 95% CI 1.01–1.84), whereas no significant association of the other five SNPs with schizophrenia was observed (Table 1). SNP3 was significantly associated with schizophrenia after Bonferroni correction (corrected $P=0.041$). We next examined the possible association between schizophrenia and genes encoding the receptors for PACAP, such as the PAC1, VPAC1 and VPAC2 receptor genes. The genotype distributions of all three SNPs in the PAC1, VPAC1 and VPAC2 genes were in Hardy–Weinberg equilibrium in both controls and patients with schizophrenia, except for that of SNP3 of the VPAC1 gene in controls (data not shown). The allele frequencies of the three SNPs in each receptor gene in the patients and controls are shown in Table 2. There was significant evidence for an association between a genetic variant of the PAC1 gene and schizophrenia (SNP2: $\chi^2=6.0$, $P=0.014$, odds ratio = 1.18, 95% CI 1.03–1.35, corrected $P=0.042$), whereas none of the SNPs in the genes encoding VPAC1 or VPAC2 was associated with schizophrenia (Table 2). The evidence that the genes encoding PACAP and its receptor PAC1 are associated with schizophrenia suggests that signaling through PACAP and PAC1 might be associated with the pathophysiology of schizophrenia.

Intermediate phenotype

As the PACAP gene has been reported to play a role in learning and memory and hippocampal long-term potentiation in rodents,[20,21] we next examined the possible impact of SNP3 of the PACAP gene, which was associated with schizophrenia, on hippocampal volume in patients with schizophrenia and controls. A genotype effect was found as bilateral reductions of hippocampal volumes (right: $P=0.04$, $t=3.2$; left: $P=0.002$, $t=4.1$) in homozygous G subjects compared with A-carriers (Figure 1a). There was also a diagnostic effect, a significant reduction in left hippocampal volume in patients with schizophrenia compared with controls ($P=0.033$, $t=3.3$). Genotype–diagnosis interaction effects on brain morphology were not found, even at a lenient threshold (uncorrected $P=0.05$). We next estimated the effects of genotypes on hippocampal volume in the control groups and schizophrenic groups, separately. Schizophrenic patients homozygous for the G allele showed a significant reduction in bilateral hippocampal volumes (right: $P=0.013$, $t=3.5$; left: $P=0.005$, $t=3.9$). On the other hand, we found significantly decreased volumes of the bilateral hippocampi in homozygous G subjects compared with the A-carriers, at a lenient threshold (uncorrected $P=0.05$) in controls; however, no voxels could survive after the correction for multiple comparisons. These data

Table 1 Allele frequencies of seven SNPs in the PACAP gene between the patients with schizophrenia and controls

SNP-ID	*dbSNP*	*Distance from SNP1*	*Major/minor polymorphism*	*Location*	*Number of subjects*		*Minor allele frequency*		P-*value*	*Odds ratio (95% CI)*
					Controls	*Patients*	*Controls*	*Patients*		
SNP1	rs2846584	—	C/T	5′-region	967	804	0.362	0.373	0.54	
SNP2	rs2231181	712	G/C	5′-UTR	960	795	0.336	0.330	0.69	
SNP3	rs1893154	1071	G/A	Intron1	951	797	0.126	0.097	0.0059	0.74 (0.59–0.92)
SNP4	rs1893153	1149	T/A	Intron1	953	793	0.174	0.163	0.37	
SNP5	rs2856966	3656	A/G	Exon3 (D54G)	953	786	0.047	0.063	0.041	1.38 (1.01–1.84)
SNP6	rs928978	4481	C/A	Intron4	958	798	0.475	0.485	0.58	
SNP7	rs1610037	6581	A/G	3′-region	962	794	0.216	0.211	0.73	

Abbreviations: CI, confidence interval; PACAP, pituitary adenylate cyclase-activating polypeptide; SNPs, single nucleotide polymorphisms.
Minor allele frequencies in controls are shown. Significant results ($P<0.05$) are indicated with underline.

Table 2 Allele frequencies of SNPs in the PAC1, VPAC1 and VPAC2 gene between the patients with schizophrenia and controls

Gene name	*SNP-ID*	*dbSNP*	*Distance from SNP1*	*Major/minor polymorphism*	*Location*	*Number of subjects*		*Minor allele frequency*		P-*value*	*Odds ratio (95% CI)*
						Controls	*Patients*	*Controls*	*Patients*		
PAC1	SNP1	rs1468687	—	T/C	Intron2	950	796	0.287	0.264	0.12	
	SNP2	rs2302475	15553	C/T	Intron5	958	797	0.479	0.520	0.014	1.18 (1.03–1.35)
	SNP3	rs2267742	34598	A/G	Intron12	936	786	0.127	0.133	0.58	
VPAC1	SNP1	rs735773	—	C/G	Intron1	937	784	0.357	0.38	0.16	
	SNP2	rs406360	12972	A/G	Intron4	948	789	0.431	0.433	0.91	
	SNP3	rs3733055	22942	G/T	Exon13 (R445L)	958	801	0.041	0.035	0.33	
VPAC2	SNP1	rs885861	—	C/T	3′-UTR	963	802	0.208	0.232	0.090	1.15 (0.98–1.36)
	SNP2	rs3793224	55026	C/T	Intron4	944	791	0.247	0.232	0.29	
	SNP3	rs3812312	109228	C/T	Intron2	923	781	0.221	0.218	0.85	

Abbreviations: CI, confidence interval; SNPs, single nucleotide polymorphisms.
Minor allele frequencies in controls are shown. Significant results ($P<0.05$) are indicated with underline.

suggest that SNP3 in the PACAP gene could have an impact on hippocampal morphology.

As the human hippocampus is related to memory function, we also examined the association between SNP3 of the PACAP gene and several subscales of the Wechsler memory scale revised version in patients with schizophrenia and controls (Figure 1b). Two-way ANCOVA on VPAI revealed significant effects of diagnosis ($F=33.8$, $P<0.0001$) and genotype of SNP3 ($F=5.2$, $P=0.024$), and an interaction between diagnosis and genotype ($F=6.6$, $P=0.011$), whereas an effect of genotype was not found in other memory subscales (data not shown). Individuals homozygous for the G allele of SNP3, which was enriched in schizophrenia, had lower scores of VPAI than schizophrenic patients carrying the A allele (Mann–Whitney *U*-test: $P=0.015$); however, there was no difference between the two genotypes in the control group ($P>0.8$). ANCOVA with gender as a covariate did not alter the statistical significance of these results in patients with schizophrenia ($P=0.029$). These data suggest that the risk SNP of the PACAP gene could be associated with reduced hippocampal volume and poorer memory performance, which are neurobiological traits related to risk for schizophrenia.

Animal study

As our data indicate that PACAP might be associated with schizophrenia, PACAP knockout mice ($PACAP^{-/-}$ mice) could be a possible animal model for schizophrenia. Several schizophrenia-related behaviors in rodents, such as hyperactivity, deficits in PPI, locomotor response to antipsychotics, disturbance in social interaction and cognitive deficits, have been commonly observed in previous pharmacological and genetic animal models for schizophrenia.[22] Therefore, we examined the impact of an atypical antipsychotic, risperidone, on hyperactivity and deficits in PPI in $PACAP^{-/-}$ mice. $PACAP^{-/-}$ mice maintained high initial levels of locomotor activity during the open field test (Figure 2a and b), as reported previously.[7] When treated with risperidone, hyperlocomotion in $PACAP^{-/-}$ mice was attenuated almost to the normal levels seen in wild-type mice; however, treatment with risperidone had no significant effect on locomotor activity in wild-type mice (Figure 2a and b). Risperidone also reversed the diminished PPI in $PACAP^{-/-}$ mice[8] to the control level seen in wild-type mice (Figure 2c). Risperidone had no significant effect on PPI levels in wild-type mice (Figure 2c) and startle amplitudes in both $PACAP^{-/-}$ and wild-type mice (data not shown). These results suggest that the abnormal behaviors in $PACAP^{-/-}$ mice, which are believed to be schizophrenia-like phenotypes in rodents, can be rescued by an atypical antipsychotic, risperidone.

The abuse of PCP, an *N*-methyl-D-aspartic acid receptor antagonist, results in positive symptoms, negative symptoms and cognitive impairments, similar to those seen in patients with schizophrenia. Thus, mice chronically treated with PCP have been used as a potential animal model for schizophrenia.[23] To assess a possible change in the expression of PACAP and PAC1 receptor in the pathological state, we performed mRNA expression analysis for PACAP and PAC1 in the frontal cortex and hippocampus of mice chronically treated with PCP. The expression level of PACAP mRNA was significantly reduced in the frontal cortex, but not in the hippocampus (Supplementary Figure 1). On the other hand, increased expression of PAC1 mRNA was observed in both frontal cortex and hippocampus (Supplementary Figure 1). Although the altered expression of PACAP and PAC1 in mouse brains treated with PCP was subtle, these data are considered to be in line with the behavioral abnormalities in $PACAP^{-/-}$ mice, a possible animal model for schizophrenia.

These results using animal models support the notion that PACAP is associated with the pathophysiology of schizophrenia.

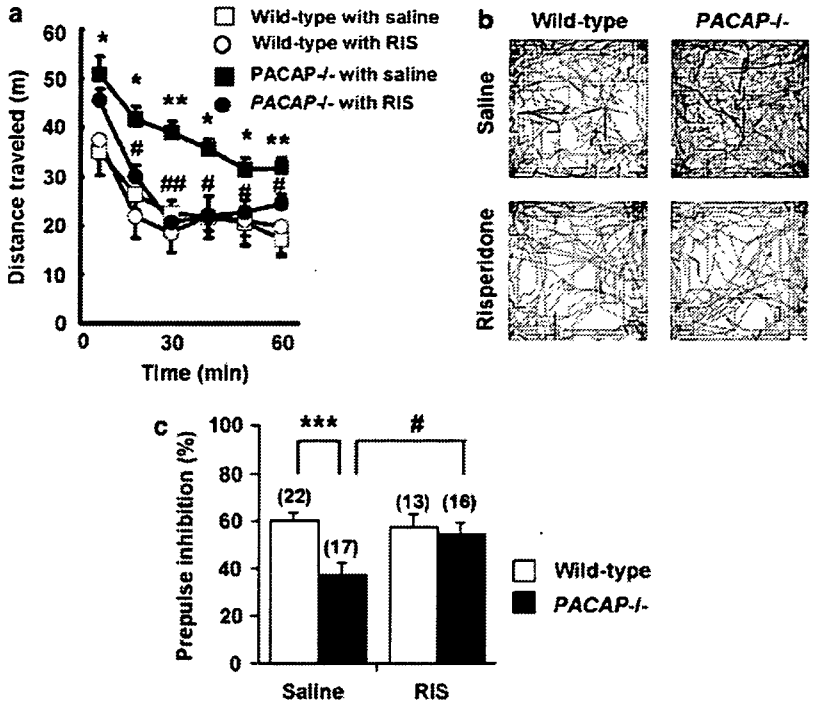

Figure 2 Hyperlocomotion and deficits in the PPI of PACAP$^{-/-}$ mice were normalized by risperidone treatment. (**a**) Locomotor activity in wild-type and PACAP$^{-/-}$ mice that received 0.1 mg/kg risperidone (RIS) or saline. $n = 6$ per group. (**b**) Representative locomotor patterns of saline- or 0.1 mg/kg risperidone-treated wild-type and PACAP$^{-/-}$ mice during 25–30 min of a 60 min recording in an open field test. (**c**) PPI levels induced by a 77 dB prepulse in wild-type and PACAP$^{-/-}$ mice after pretreatment with risperidone (0.1 mg/kg) or saline. Numbers of animals for experiments are shown in parentheses. Data are given as means ± s.e.m. $^{*}P<0.05$, $^{**}P<0.01$, $^{***}P<0.001$, compared to wild-type. $^{\#}P<0.05$, $^{\#\#}P<0.01$, compared with saline in PACAP$^{-/-}$ mice.

Discussion

Our findings support the possibility that PACAP is a potential schizophrenia susceptibility gene. Clinical association between schizophrenia and the genes encoding PACAP and PAC1 and an association between intermediate phenotypes, hippocampal volume and visual associate memory performance and a risk SNP in the PACAP gene have been demonstrated in our study. There are several limitations in our results. We screened control subjects with no past or current visits to psychiatric services; however, we could not exclude the possibility that they have an undiagnosed or untreated psychiatric disorder. The obtained evidence for association was not very strong, especially in the association between the genotype and visual associate memory performance ($P<0.05$ level). When we applied corrections for multiple testing for several memory tests, this positive association became negative. This association is not conclusive, although the association between the risk allele for schizophrenia and poorer memory performance might be attractive. Thus, replication studies should be conducted to confirm our findings. We do not know whether SNP3 alters the expression/function of the PACAP gene. Accordingly, there remains the possibility that other polymorphisms, which are in linkage disequilibrium to this polymorphism, are truly responsible for giving susceptibility.

Studies aiming to identify susceptibility genes for schizophrenia are faced with the confounds of subjective clinical criteria and the likelihood of allelic and locus heterogeneity. Although schizophrenia is substantially heritable, the mode of inheritance is complex, involving numerous genes of small effect and a nontrivial environmental component. The concept of intermediate phenotype (endophenotype) assumes that neurobiological deficits occur across the schizophrenia spectrum in schizophrenia patients, schizotypal patients and clinically unaffected relatives of schizophrenia patients. The intermediate phenotype approach is an alternative method for measuring phenotypic variation that may facilitate the identification of susceptibility genes in the context of complexly inherited traits. Using this approach, we showed an association between the PACAP gene and two intermediate phenotypes, hippocampal volume and visual associate memory, in addition to the genetic association with schizophrenia. Our study could be a successful example of using this strategy to find susceptibility genes for complex diseases.

The hyperactivity and deficits in PPI observed in PACAP$^{-/-}$ mice[7,8] are believed to be schizophrenia-like behaviors in rodents. PAC1 knockout mice also show abnormal behaviors, including elevated locomotor activity and abnormal social behavior.[24,25] Our genetic findings, which demonstrate an association

between schizophrenia and two genes, PACAP and PAC1, are supported by the abnormal behaviors in knockout mice of PACAP and PAC1. Risperidone, an atypical antipsychotic, has the advantage of better extrapyramidal tolerability than conventional antipsychotics, but also has advantages in cognitive disturbances and the treatment of negative and depressive symptoms.[26] Our previous study showed that haloperidol, a representative conventional antipsychotic, rescued hyperactivity,[7] but did not rescue deficits in PPI.[8] As risperidone treatment rescued both of these abnormalities in PACAP$^{-/-}$ mice, and as risperidone is a combined D2 and 5-HT$_{2A}$ receptor antagonist, either dopamine or serotonin signaling, or both, could be relevant to the abnormal behaviors in PACAP$^{-/-}$ mice.

Our convergent evidence suggests that investigation of PACAP-PAC1 signaling in the brain could provide a clue to elucidating the possible mechanisms of pathophysiology in schizophrenia.

Acknowledgments

We thank Ms Tomoko Shizuno, Keiko Okada and Akiko Murakami for technical assistance and staff of the National Center of Neurology and Psychiatry for recruiting patients and healthy subjects. This work was supported in part by Grants-in-Aid from the Japanese Ministry of Health, Labor and Welfare (H18-kokoro-005, H17-kokoro-001, H17-kokoro-007 and H16-kokoro-002); the Japanese Ministry of Education, Culture, Sports, Science and Technology; Japan Society for the Promotion of Science; CREST (Core Research for Evolutional Science and Technology) of JST (Japan Science and Technology Agency); Japan Foundation for Neuroscience and Mental Health; the Sankyo Foundation of Life Science; and Taisho Pharmaceutical Co Ltd.

References

1 Owen MJ, Williams NM, O'Donovan MC. The molecular genetics of schizophrenia: new findings promise new insights. *Mol Psychiatry* 2004; **9**: 14–27.
2 Preston GA, Weinberger DR. Intermediate phenotypes in schizophrenia: a selective review. *Dialog Clin Neurosci* 2005; **7**: 165–179.
3 Braff DL, Light GA. The use of neurophysiological endophenotypes to understand the genetic basis of schizophrenia. *Dialog Clin Neurosci* 2005; **7**: 125–135.
4 Hashimoto H, Shintani N, Baba A. Higher brain functions of PACAP and a homologous Drosophila memory gene amnesiac: insights from knockouts and mutants. *Biochem Biophys Res Commun* 2002; **297**: 427–431.
5 Vaudry D, Gonzalez BJ, Basille M, Yon L, Fournier A, Vaudry H. Pituitary adenylate cyclase-activating polypeptide and its receptors: from structure to functions. *Pharmacol Rev* 2000; **52**: 269–324.
6 Arimura A. Perspectives on pituitary adenylate cyclase activating polypeptide (PACAP) in the neuroendocrine, endocrine, and nervous systems. *Jpn J Physiol* 1998; **48**: 301–331.
7 Hashimoto H, Shintani N, Tanaka K, Mori W, Hirose M, Matsuda T *et al.* Altered psychomotor behaviors in mice lacking pituitary adenylate cyclase-activating polypeptide (PACAP). *Proc Natl Acad Sci USA* 2001; **98**: 13355–13360.
8 Tanaka K, Shintani N, Hashimoto H, Kawagishi N, Ago Y, Matsuda T *et al.* Psychostimulant-induced attenuation of hyperactivity and prepulse inhibition deficits in Adcyap1-deficient mice. *J Neurosci* 2006; **26**: 5091–5097.
9 Nurnberger Jr JI, Foroud T. Genetics of bipolar affective disorder. *Curr Psychiatry Rep* 2000; **2**: 147–157.
10 Ishiguro H, Ohtsuki T, Okubo Y, Kurumaji A, Arinami T. Association analysis of the pituitary adenyl cyclase activating peptide gene (PACAP) on chromosome 18p11 with schizophrenia and bipolar disorders. *J Neural Transm* 2001; **108**: 849–854.
11 Hashimoto R, Suzuki T, Iwata N, Yamanouchi Y, Kitajima T, Kosuga A *et al.* Association study of the frizzled-3 (FZD3) gene with schizophrenia and mood disorders. *J Neural Transm* 2005; **112**: 303–307.
12 Hashimoto R, Okada T, Kato T, Kosuga A, Tatsumi M, Kamijima K *et al.* The breakpoint cluster region gene on chromosome 22q11 is associated with bipolar disorder. *Biol Psychiatry* 2005; **57**: 1097–1102.
13 Good CD, Johnsrude IS, Ashburner J, Henson RN, Friston KJ, Frackowiak RS. A voxel-based morphometric study of ageing in 465 normal adult human brains. *Neuroimage* 2001; **14**: 21–36.
14 Ashburner J, Friston KJ. Voxel-based morphometry – the methods. *Neuroimage* 2000; **11**: 805–821.
15 Pezawas L, Verchinski BA, Mattay VS, Callicott JH, Kolachana BS, Straub RE *et al.* The brain-derived neurotrophic factor val66met polymorphism and variation in human cortical morphology. *J Neurosci* 2004; **24**: 10099–10102.
16 Mechelli A, Friston KJ, Frackowiak RS, Price CJ. Structural covariance in the human cortex. *J Neurosci* 2005; **25**: 8303–8310.
17 Maldjian JA, Laurienti PJ, Kraft RA, Burdette JH. An automated method for neuroanatomic and cytoarchitectonic atlas-based interrogation of fMRI data sets. *Neuroimage* 2003; **19**: 1233–1239.
18 Sakaue M, Ago Y, Baba A, Matsuda T. The 5-HT1A receptor agonist MKC-242 reverses isolation rearing-induced deficits of prepulse inhibition in mice. *Psychopharmacology (Berl)* 2003; **170**: 73–79.
19 Chiba S, Hashimoto R, Hattori S, Yohda M, Lipska B, Weinberger DR *et al.* Effect of antipsychotic drugs on DISC1 and dysbindin expression in mouse frontal cortex and hippocampus. *J Neural Transm* 2006; **113**: 1337–1346.
20 Matsuyama S, Matsumoto A, Hashimoto H, Shintani N, Baba A. Impaired long-term potentiation *in vivo* in the dentate gyrus of pituitary adenylate cyclase-activating polypeptide (PACAP) or PACAP type 1 receptor-mutant mice. *Neuroreport* 2003; **14**: 2095–2098.
21 Sacchetti B, Lorenzini CA, Baldi E, Bucherelli C, Roberto M, Tassoni G *et al.* Pituitary adenylate cyclase-activating polypeptide hormone (PACAP) at very low dosages improves memory in the rat. *Neurobiol Learn Mem* 2001; **76**: 1–6.
22 Gainetdinov RR, Mohn AR, Caron MG. Genetic animal models: focus on schizophrenia. *Trends Neurosci* 2001; **24**: 527–533.
23 Jentsch JD, Roth RH. The neuropsychopharmacology of phencyclidine: from NMDA receptor hypofunction to the dopamine hypothesis of schizophrenia. *Neuropsychopharmacology* 1999; **20**: 201–225.
24 Otto C, Martin M, Wolfer DP, Lipp HP, Maldonado R, Schutz G. Altered emotional behavior in PACAP-type-I-receptor-deficient mice. *Brain Res Mol Brain Res* 2001; **92**: 78–84.
25 Nicot A, Otto T, Brabet P, Dicicco-Bloom EM. Altered social behavior in pituitary adenylate cyclase-activating polypeptide type I receptor-deficient mice. *J Neurosci* 2004; **24**: 8786–8795.
26 Moller HJ. Risperidone: a review. *Expert Opin Pharmacother* 2005; **6**: 803–818.

Supplementary Information accompanies the paper on the Molecular Psychiatry website (http://www.nature.com/mp)

Available online at www.sciencedirect.com
ScienceDirect
Neuroscience Letters 412 (2007) 195–200
Neuroscience Letters
www.elsevier.com/locate/neulet

A new gain-of-function allele in chimpanzee tryptophan hydroxylase 2 and the comparison of its enzyme activity with that in humans and rats

Kyung-Won Hong[a], Yuko Sugawara[b], Hiroyuki Hasegawa[b], Ikuo Hayasaka[c], Ryota Hashimoto[d,e], Shin'ichi Ito[f], Miho Inoue-Murayama[f,*]

[a] *The United Graduate School of Agricultural Science, Gifu University, Gifu 501-1193, Japan*
[b] *Department of Biosciences, Teikyo University of Science and Technology, Yamanashi 409-0193, Japan*
[c] *Sanwa Kagaku Kenkyusho Co. Ltd., Uki 869-3201, Japan*
[d] *The Osaka-Hamamatsu Joint Research Center for Child Mental Development, Osaka University Graduate School of Medicine, Suita 565-0871, Japan*
[e] *Department of Psychiatry, Osaka University Graduate School of Medicine, Suita 565-0871, Japan*
[f] *Faculty of Applied Biological Sciences, Gifu University, Gifu 501-1193, Japan*

Received 6 September 2006; received in revised form 5 October 2006; accepted 3 November 2006

Abstract

Tryptophan hydroxylase 2 (TPH2) is a rate-limiting enzyme of neuronal serotonin biosynthesis. Recently, two single nucleotide polymorphisms (SNPs) at the exon 11 coding region that resulted in amino acid substitutions in the C-terminal domain have been reported to affect enzyme activity in humans and mice. We determined 175 base-pair sequences of the exon 11 region in nine primate species from all recognized lineages. All nucleotide sequence substitutions were synonymous, with the exception of one adenine (A) to guanine (G) substitution at the 1404th position in the open reading frame (ORF). This substitution leads to a glutamine (Q) to arginine (R) amino acid substitution at the 468th position within chimpanzee sequences. The frequency of the *G* allele was 0.24 among 66 chimpanzees. Therefore, it is a novel SNP observed in chimpanzees, and we have named these two alleles as *ch468Q* and *ch468R*, respectively. When expressed in HeLa cells, *ch468R* caused an approximate 20% increase in enzyme function during L-5-hydroxytryptophan (5HTP) production ($P < 0.001$). We also surveyed the interspecies difference in enzyme activity among human, chimpanzee, and rat. Although the rat showed an identical amino acid sequence at the C-terminal region as those of human and *ch468Q*, the rat enzyme was more active than those of human or chimpanzee ($P < 0.001$), indicating the importance of substitutions in other regions. Our findings on the chimpanzee SNP will be a useful genetic marker in understanding the individual difference in the serotonin-related behavior.
© 2006 Elsevier Ireland Ltd. All rights reserved.

Keywords: TPH2; SNP; 5HTP; Chimpanzee; Serotonin

Serotonin synthesis is mediated by the rate-limiting enzyme tryptophan hydroxylase (TPH), which catalyzes the pterin-dependent hydroxylation of L-tryptophan to L-5-hydroxytryptophan (5HTP). Additionally, this reaction is the first step in the synthesis of melatonin, which is involved in the regulation of mammalian reproduction and circadian rhythms [27]. The TPH belongs to the family of tetrahydrobiopterin-dependent aromatic amino acid hydroxylases, which includes phenylalanine hydroxylase (PAH) and tyrosine hydroxylase (TH) [14]. These enzymes share similar protein organization composed of a regulatory N-terminal domain, a catalytic domain, and a short C-terminal oligomerization domain (Fig. 1a) [6–8]. Although the precise manner is often unique for each hydroxylase, they can be activated by similar mechanisms [4,9,10].

Recently, TPH isoform 2 was discovered to be preferentially located in brain dorsal raphe [23,28] and in the peripheral myenteric neurons in the gut [4]. The discovery of TPH2 has renewed great interest in studying the role of this enzyme in the neurochemical function of serotonin. To date, over 500 single nucleotide polymorphisms (SNPs) have been identified in the TPH2 gene in humans and mice, but coding non-synonymous SNPs are only six [3,33]. A number of recent studies have

* Corresponding author. Tel.: +81 58 293 2874; fax: +81 58 293 2874.
E-mail address: miho-i@gifu-u.ac.jp (M. Inoue-Murayama).

0304-3940/$ – see front matter © 2006 Elsevier Ireland Ltd. All rights reserved.
doi:10.1016/j.neulet.2006.11.010

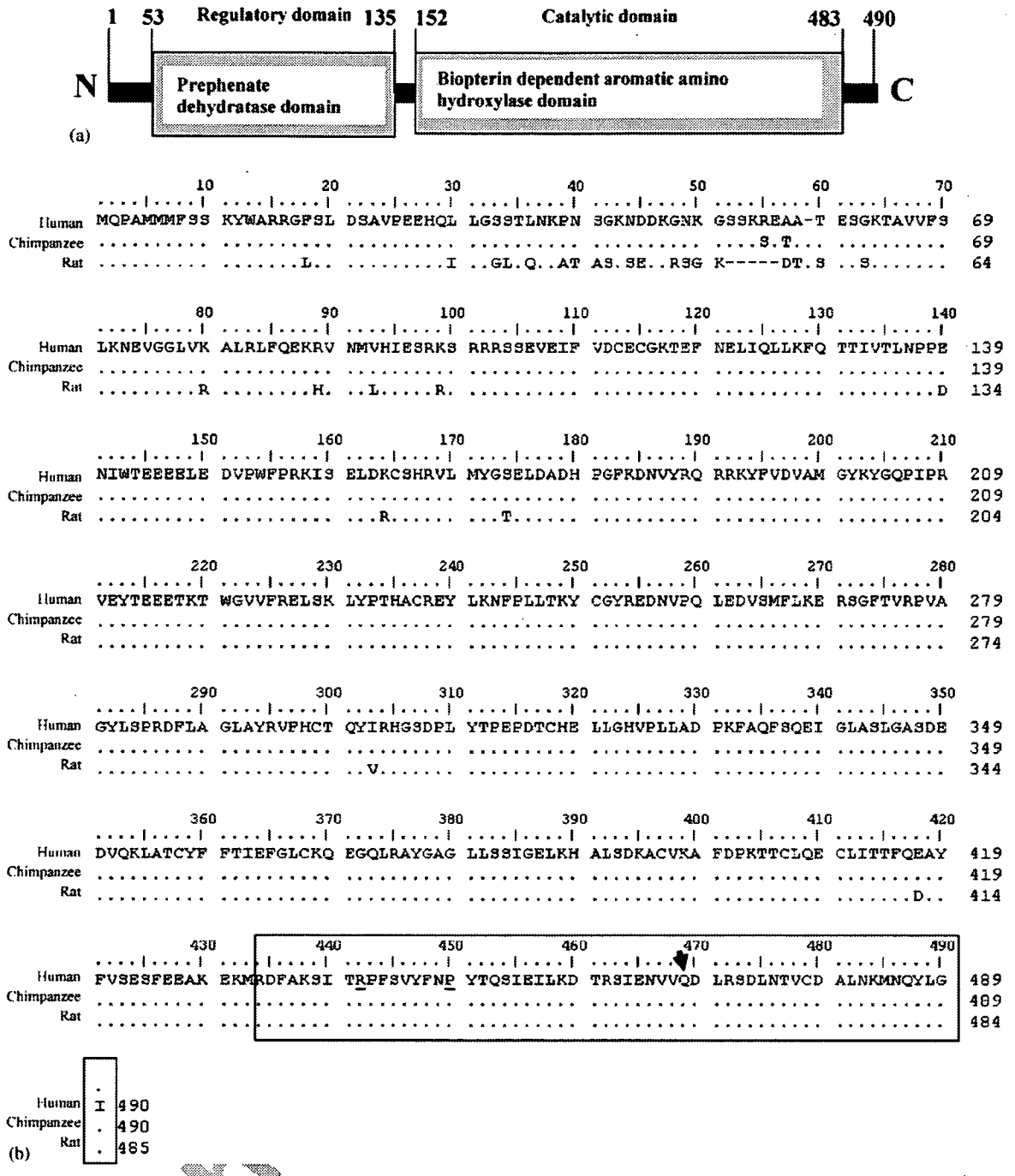

Fig. 1. The schematic TPH2 structure and amino acid sequence alignment. (a) The schematic TPH2 structure including two functional domains. The numbers indicate the amino acid position based on the human coding region. (b) The amino acid alignments of three mammals. The sequenced region (corresponding exon 11 coding region) of primate species is boxed and the chimpanzee-specific Q468R polymorphic site is indicated by an arrowhead. Polymorphic sites in humans (R441H) and mice (P447R) are underlined. Accession numbers of human, chimpanzee, and rat are NP_775489, XP_522470, and NP_776211, respectively.

already reported the association between genetic polymorphisms and affective disorder and suicidal tendency [3,9,24,34]. Additionally, a number of interesting differences in the properties of TPH1 and TPH2 have been revealed, suggesting that these enzymes may have different catalytic control mechanisms or are differentially regulated at the post-translational level [19].

In human and mouse studies, SNPs in TPH2 have been suggested to alter enzyme function [31,32]. The human TPH2 contained an SNP that replaced a wild-type arginine with a histidine (R441H). Expression of the mutant TPH2 in PC12 cells resulted in an approximate 80% decrease in serotonin levels as compared to the wild-type. R441H mutants were identified in unipolar major depression patients. In the mouse TPH2, a wild-type proline has been reported to be replaced by arginine (P447R mutant). Expression of mutant TPH2 revealed an approximate 55% decrease in serotonin levels as compared to wild-type. The mutant P447R homozygous inbred strains (BALB/c and DBA/2J) of mice showed 50–70% decrease in the rate of serotonin synthesis in the brain when compared to the wild-type homozygous strains (C57BL/6 and 129X1/SvJ). Interestingly,

the mice from these strains display significantly different aggressive behavior [16] and responses to antidepressants [2,18]. These results raised the possibility that similar mutations in nonhuman primates may affect their brain serotonin levels.

In general, the nucleotides and amino acids similarities among the TPH2 sequences of human, chimpanzee, and rat that were downloaded from GenBank database were >80% and >90%, respectively. The C-terminal region (highlighted by a box) was identical among the major allele of the species except for a proline to arginine replacement in mouse and for an arginine to histidine replacement in human (Fig. 1a and b).

The close genetic, physiological, and behavioral similarities between humans and nonhuman primates provide the basis for a comparative analysis of the genetic and environmental factors underlying both normative and pathological outcomes in behavioral development [1]. In this study, our primary purpose was to identify a new polymorphic loci in chimpanzees neurotransmitter related genes. Therefore, we sequenced the exon 11 coding region that corresponds to the polymorphic regions in humans and mice for several primate species.

Genomic DNA was extracted from the peripheral blood or buccal mucous membrane obtained from humans (healthy Japanese subjects, $n = 10$; informed consent was obtained in accordance with the guidelines of Gifu University), chimpanzees (*Pan troglodytes*, $n = 66$), gorillas (*Gorilla gorilla*, $n = 10$), orangutans (*Pongo pygmaeus*, $n = 10$), agile gibbons (*Hylobates agilis*, $n = 5$), Japanese macaques (*Macaca fuscata*, $n = 4$), mandrill (*Papio sphinx*, $n = 1$), common marmosets (*Callithrix jacchus*, $n = 3$), tarsier (*Tarsius bancanus*, $n = 1$), and galago (*Galago crassicaudatus*, $n = 1$). Thus, all primate lineages were covered. Most of the nonhuman primate samples were obtained from the Primate Research Institute of Kyoto University and Sanwa Kagaku Kenkyusho Co. Ltd.

We determined the sequences in 10 individuals of chimpanzees and each one individual for the other species. PCR was performed for the amplification of a 295 bp sequence including 175 bp of the exon 11 coding region. Ten microliters of the reaction mixture containing 20 ng DNA, 0.5 μM of each primer, 0.5 U *LA Taq* polymerase, GC buffer I (TaKaRa, Shiga, Japan), and 400 μM of each dNTP was used. The primer sequences employed were 5′-TTCTGTTTATTCTGCAGGGACT-3′ (TPH2F) and 5′- TTAGCCAAGCCATGACACAG-3′ (TPH2R), corresponding to intron 10 and 3′UTR of the human TPH2 genomic sequence. After an initial incubation at 95 °C for 2 min, PCR amplification was performed for 35 cycles consisting of 95 °C for 30 s, 60 °C for 1 min and 74 °C for 2 min; this was followed by a final extension at 74 °C for 10 min. The PCR products were purified by using a PCR purification kit (Roche, Mannheim, Germany), followed by sequencing of both strands at least twice by using an ABI 3100 DNA sequencer (Applied Biosystems, Foster City, CA) according to manufacturer's instructions.

The nucleotide sequences of the C-terminal domain (exon 11 coding region of TPH2) in the nine primate species are shown in DDBJ database with accession numbers AB68316–AB68324. A total of 23 nucleotide substitutions were observed. All substitutions were silent, except one substitution within chimpanzees. An adenine (A) at the 1404th position was substituted by guanine (G), and this change caused a replacement of the 468th glutamine (CAG, *ch468Q*) by arginine (CGG, *ch468R*). Both chimpanzee sequences contained one substitution synonymous with that of human sequence at the 1468th position.

Genotyping for the chimpanzee SNP for remaining 56 individuals was performed by using a PCR-RFLP method. After amplification using TPH2F and TPH2R primers, 1 μl of the PCR product was incubated at 37 °C overnight in the reaction mixture having a total volume of 10 μl, containing 1 × NEBuffer 4 with 1.5 U of *HpyCH4*V (New England BioLabs, Beverly, MA). The products were subsequently separated by electrophoresis on a 2.0% agarose gel.

The allelic frequency of *G* allele among 66 chimpanzees was 0.24. The genotypic frequencies of *G/G*, *A/A*, and *G/A* were 0.091, 0.606, and 0.303, respectively. The presence of Hardy–Weinberg equilibrium was examined by using the Chi-square test for goodness of fit. The observed genotypic frequency distribution well accorded with the expectation under the Hardy–Weinberg equilibrium (Chi-square test, $P = 0.364$). To confirm the chimpanzee specificity of the SNP, we also conducted the SNP genotyping in each of the 10 humans, 10 gorillas, 10 orangutans, five agile gibbons, four Japanese macaques, and three common marmosets, but we could not detect the same substitution. If these species have the SNP site in the same frequency as chimpanzee, then it should be detected by the possibility of 99.9% in 10 individuals [15]. For confirmation, we need to survey larger sample size and diverse population.

For elucidating the functional effect of chimpanzee SNP, the human full-length ORF was amplified from the human brain hippocampus cDNA library (TaKaRa, Shiga, Japan) by using the primers 5′-CCCTGCTGCAGAGAAAGAAT-3′ (TPH2Fm) and 5′- AGATCATGCTGGCAACAACA-3′ (TPH2Rm), and was subsequently ligated into a human TPH2/TOPO TA cloning vector (Invitrogen, Carlsbad, CA). The chimpanzee amino acid sequence differed from that of the humans at only three positions. Of these, the two positions – C164A (R54S) and G170A (A56T) – were common in all the chimpanzees surveyed, but the A1404G (Q468R) substitution was polymorphic within chimpanzees. Therefore, two types of chimpanzee TPH2 ORFs were obtained by the mutagenesis of human ORF. The following are the oligonucleotides used to generate the ch468Q and ch468R (lowercase underlined letters represent new codons introduced by site-directed mutagenesis): 5′-AGCAAAagtGAAactGCTACCGAAAG-3′ for R54S and A56T, and 5′-ATGTGGTGcggGACCTTCGCAG-3′ for Q468R.

The rat ORF was amplified by 5′-TCCCCGCGGTTCGAAACCatgcagcccgcaatgatgat-3′ (ratTPH2Fm) and 5′-GGACTAGTCTAGAtcaaatccccaaatattggttcatt-3′ (ratTPH2Rm). The ratTPH2Fm included *Csp45*I restriction sites and a ribosome-binding sequence (ACC) flanking the 5′ region of the TPH2 ORF, and the ratTPH2Rm included the *Xba*I restriction sites flanking the 3′ region of the rat TPH2 ORF.

The human and chimpanzee inserts were obtained by digestion with *Kpn*I and *Not*I, the recognition sites of which were located on the TOPO TA cloning vector, and the rat insert

was obtained by digestion with *Csp*45I and *Xba*I. The inserts were then ligated with the Gateway® pENTR™11 entry vector (Invitrogen, Carlsbad, CA) digested with the same restriction enzymes. The inserts were transferred from the entry vector to the Gateway™ pDEST™ 12.2 destination vector (Invitrogen, Carlsbad, CA) by an LR reaction with Gateway® LR Clonase™ II Enzyme Mix (Invitrogen, Carlsbad, CA).

Transfection of pDEST12.2/TPH2 ORFs to HeLa cells was performed using jet PEI® (PolyPlus-Transfection, Illkirch, France) essentially according to the manufacturer's instructions. HeLa cells (2×10^5 cells/3.5 cm dish) were plated 28 h prior to the treatment. The cells were transfected with 1.7 μg DNA (1.5 μg of TPH2/pDEST12.2 and 0.2 μg of β-GAL/pCMV-SPORT) plus 3.4 μl jet PEI for 48 h.

After transfection of the expression vectors for 48 h, HeLa cells were collected and the TPH activity was determined essentially as described previously [11]. Cells in the monolayer culture were collected in PBS(−) "Ca/Mg-free PBS" and then subjected twice to freezing in liquid nitrogen and thawing on water. The disrupted cells were pre-incubated for 15 min at 30 °C in 0.1 M Tris–HCl (pH 8.0) containing 30 mM DTT, 50 μM $Fe(NH_4)_2(SO_4)_2$, and 4 mg/ml catalase in a total volume of 100 μl. Subsequently, 50 μl of another cocktail was added to yield a final reaction mixture of 250 μM tryptophan, 400 μM 6R-tetrahydrobiopterin, 500 μM NADH, 1 mM NSD-1015, 2 mg/ml catalase, and 50 μg/ml dihydropteridine reductase in 0.1 M K-phosphate buffer (pH 6.9). The enzyme reaction was allowed to proceed for 10 min at 30 °C and was then terminated by adding 1 M perchloric acid.

The 5HTP formed was measured using a high performance liquid chromatography (HPLC) system equipped with a fluorescence monitor (JASCO model, FP920) set at excitation and emission wave lengths of 302 nm and 350 nm, respectively. The solid phase was ODS (4.6 mm × 250 mm, JASCO, Finepak SIL-C18T5), the mobile phase was a 100:5:7 mixture of 40 mM sodium acetate (adjusted to pH 3.5 with formic acid): acetonitrile: methanol and the flow rate was 1 ml/min [10]. To correct the enzyme activity, we employed the β-galactosidase enzyme assay system (Promega, Madison, WI) according to manufacturer's instructions.

Statistical analysis of enzyme activity was performed with one-way ANOVA followed by Tukey post hoc comparison. All *P*-values reported were two tailed. Statistical significance was defined at $P < 0.05$.

We measured the TPH2 enzyme activity to estimate the production of L-5-hydroxytryptophan (5HTP) in *ch468Q*, *ch468R*, human, and rat. The results of the enzyme activity assay were 49.40 ± 0.45 pmole/10 min/β-gal mU in *ch468Q*, 64.36 ± 1.67 pmole/10 min/β-gal mU in *ch468R*, 50.11 ± 1.72 pmole/10 min/β-gal mU in human, and 65.32 ± 0.99 pmole/10 min/β-gal mU in rat (Fig. 2). The *ch468R* and rat isoform showed significantly higher activity than *ch468Q* and human isoform (ANOVA, $P < 0.05$).

The sequences of the exon 11 coding region were well conserved among human and nonhuman primate species, except one missense substitution at A1404G leading to Q468R in chimpanzees. The enzyme activity assay indicated that the capacity

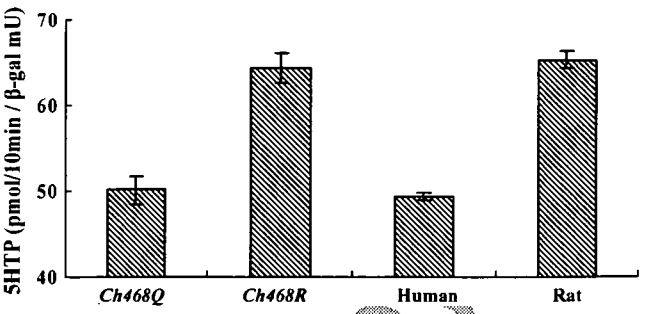

Fig. 2. Inter- and intra-specific comparisons of TPH2 activity. The TPH2 activity assay was conducted *in vitro* with disrupted cells of transfected HeLa cells and expressed as pmoles of 5-hydroxytryptophan (5HTP) per 10 min per β-gal mU. All data are presented as mean ± S.D.

of L-5-hydroxytrytophan biosynthesis was the same in *ch468Q* and human TPH2, whereas it was significantly high in the case of *ch468R*. If there were no significant changes in TPH2 expression levels, it could be a new gain-of-function allele. Although the molecular mechanism by which the *Q468R* mutation enhances catalytic function was not elucidated in the present study, replacement of the non-polar glutamine by the positively charged arginine could suggest the influence of the conformation of the catalytic site of the enzyme in some way [26].

This is the first comparative study on human and rat enzyme activity. In mice, *in vitro* 5HTP synthesis corresponded to their brain serotonin levels [31]. Therefore, although the difference in the activity was produced by an *in vitro* analysis, the high level of rat TPH2 activity probably implies the genetically higher serotonin concentration in serotonergic neurons of rodents than in human and nonhuman primates, if there were no significant differences in the amount of TPH2 protein.

TPH2, similar to all other monoamine-oxygenases, assembles into tetramers [29,30], and the tetramerization domain is present mostly within a 24-residue α-helix in the extreme C-terminal region of the enzymes [4,5]. The region of exon 11 is a part of the biopterin-dependent aromatic amino acid hydroxylase domain and also contains the tetramerization domain. The chimpanzee Q468R substitution is located on the tetramerization domain of the C-terminal. Therefore, the chimpanzee SNP may influence tetramer formation.

This result implies that low enzyme activity in humans and chimpanzees may result in low serotonin concentrations in the brain and may influence differences in the behavioral traits among chimpanzees as observed in mice [31,32]. Neurotransmitters such as dopamine and serotonin have been the prime target for understanding the biological basis of animal behaviors and interactions among animal groups. Primate social colonies are very sophisticated, and social interactions of chimpanzees are an interesting target for anthropologists. However, few genetic markers were reported for understanding primate behavioral traits [1,22].

In this study, we discovered a functional genetic marker for understanding the relationship between serotonin and chimpanzee behaviors including social dominance or aggression. The previous primate studies on the relationship between the serotonergic system and social dominance and aggression were

Author's personal copy